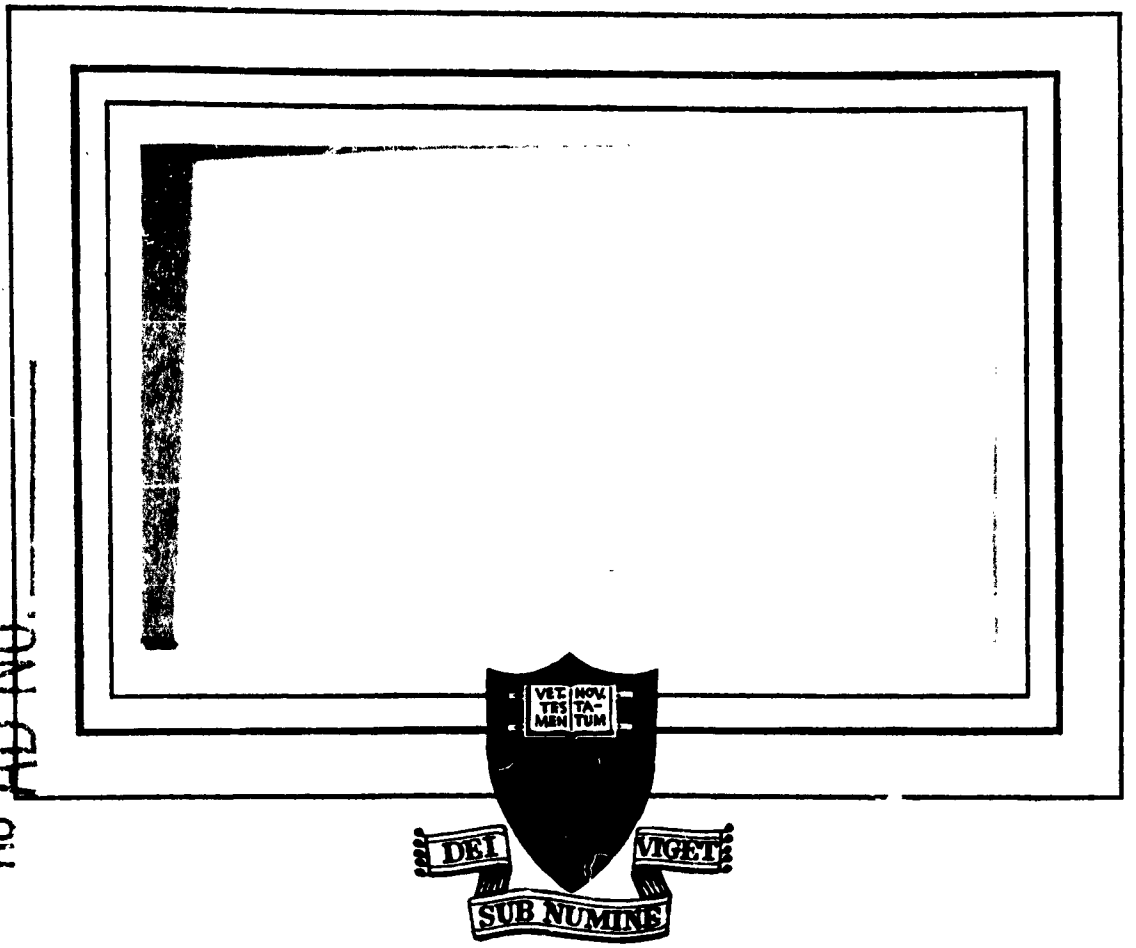

PRINCETON UNIVERSITY

DEPARTMENT OF AERONAUTICAL ENGINEERING

DEPARTMENT OF THE NAVY
OFFICE OF NAVAL RESEARCH
(ADVANCED RESEARCH PROJECTS AGENCY)

Contract Nonr 1858(32) - NR 098-201
(ARPA Order No. 23-59; 23-60 Amend. 5)

A Technical Report On

COMPARISON OF SOLID PROPELLANT BURNING RATES IN STRANDS AND ROCKET MOTORS

Aeronautical Engineering Laboratory Report No. 556

Prepared by: Clarke E. Hermance
Clarke E. Hermance
Research Aide

Approved by: Martin Summerfield
Martin Summerfield
Professor of Jet Propulsion

May 1961

Department of Aeronautical Engineering
PRINCETON UNIVERSITY
Princeton, New Jersey

ACKNOWLEDGMENTS

I wish to thank the many people who through their advice, guidance, and technical help, made this thesis possible.

The financial support for this research project (except for my own fellowship) was assumed by the Office of Naval Research, mainly through an ONR-ARPA Contract No. 1858 (32), and in small part through Project SQUID Contract No. NONR 1858 (25), NR-098-038.

Mr. E. Karl Bastress and Mr. David W. Blair, graduate students with whom I was privileged to work, provided many of the procedures and developments used in this research as well as very helpful advice and encouragement. The technique of determining burning rates from strands is largely due to the work of David W. Blair.

Much is owed to Mr. Michael Gula for his invaluable help in the making of propellant and in conducting rocket motor firing tests, and to Mr. E. R. Crosby for his help in the photography needed in this thesis.

The Jet Propulsion Staff of the Forrestal Research Center was of great assistance in the design, material procurement, and construction of the necessary experimental apparatus.

Dr. Kimball P. Hall--a great source of valuable information on material properties of solid propellants and on safety procedures--must receive special thanks for his advice and interest in this project.

To the Department of Mechanical Engineering for their financial support, and especially Professor Robert M. Drake, Jr., Chairman, for his great encouragement and help, I wish to express my deepest gratitude. I was supported in the course of this work by a Henry Crathorne Phillips Fellowship from the Mechanical Engineering Department.

Finally, for direction of this research program, for providing invaluable advice, and for his readiness to discuss technical problems, I express great appreciation to Professor Martin Summerfield, of the Aeronautical Engineering Department, with whom I have had the privilege to work.

ABSTRACT

The purposes of this research were to investigate the burning rate of a composite, solid propellant in a rocket motor and to perform a comparison with results of the earlier Princeton research on the burning rate of a strand of composite, solid propellant which led to a theoretical burning rate law. The role of radiative energy feedback to the propellant surface was of special interest in this research.

A rocket motor incorporating interchangeable grains, and interchangeable nozzles, which allowed progressive burning between various pressure levels, was developed. Chamber pressure versus time was recorded during each motor firing. By equating the rate of production of combustion products from the solid propellant to the flow rate of combustion products out of the nozzle an instantaneous burning rate for an instantaneous chamber pressure was calculated. It was found that, in general, the burning rate in the rocket motor at any specified pressure was less than that of a strand burning at the same pressure. A detailed investigation of the reasons for this unexpected behavior has been initiated, but with no definitive results as yet.

The energy feedback due to the presence of radiative heat flux, and its effect on the burning rate in a rocket motor, was investigated. In particular, the radiation flux from the central gas column incident upon the propellant surface was theoretically computed. The values obtained proved to be of the same order of magnitude as the measured radiation flux from the active flame zone. However, preliminary experimental results showed the radiation flux from the hot gas column to the propellant surface to be approximately twice that received from the flame zone. This radiative feedback was expected to make the burning

rate in a rocket motor higher than that of a strand at the same pressure. As noted above, this was opposite to the experimental result.

It is concluded that more exact measurement of the burning rates, particularly in a rocket motor at constant pressure, should be made. At this point, there are only two possibilities to explain the burning rate discrepancy noted: one, a fundamental difference between large, enclosed flames and small, open flames not yet disclosed in the current analysis; two, an unidentified error associated with the determination of burning rates. The next step should be to check the latter possibility.

TABLE OF CONTENTS

TABLE OF CONTENTS (Continued)

LIST OF FIGURES

LIST OF FIGURES

CHAPTER I

INTRODUCTION AND OBJECTIVES OF THE RESEARCH

I. Summerfield Burning Rate Theory of Composite, Solid Propellants: Early Tests and Results.

Early research on the properties of burning solid propellants revealed that the burning rate was a function of the gas pressure to which the propellant was subjected. Initially, double-base propellants were used and studied, and a fairly complete understanding of their combustion process was obtained. Double-base propellants are a homogeneous mixture of nitrocellulose and nitroglycerine. Later, composite propellants consisting of a fuel matrix acting as a binder for solid crystals of oxidizer evenly distributed in the formulation were developed. Several empirical burning rate laws such as Muraour's Law ($r = a + bp$), St. Robert's Law ($r = bp^n$ where $0.3 \leq n \leq 0.7$) and a combination of the two ($r = a + bp^n$) were applied but were found to be valid for composite propellant combustion only over short pressure ranges. This situation meant that many tests had to be made in order to obtain even an empirical description of the burning rate-pressure relationship for any particular propellant -- a very time consuming task. In order to fill the void of understanding concerning composite propellant combustion and to determine a burning rate law applicable over a wide pressure range, Professor Martin Summerfield proposed a so-called granular diffusion flame model for composite, solid propellant combustion. The relationship resulting from this model was tested with solid propellant strand data and found to agree very well with the experimental results (1). This relationship is of the form:

$$1/r = a/p + b/p^{1/3}$$

In the above equation, (a) is a constant determined by the chemical kinetics of the combustion which are rate-controlling at low pressures, and (b) is a constant determined by the diffusion characteristics of the fuel and oxidizer vapors, which are rate-controlling for combustion at high pressures (1).

II. Experimentally Noted Differences in Rocket Motor and Strand Burning Rates

A strong test of any composite, solid propellant burning rate law is how well it predicts the burning rate as a function of pressure in actual application. Prediction of burning rates of composite propellant strands using the Summerfield granular diffusion flame theory of combustion was indeed accurate when compared with the experimental results obtained from burning strands. The accuracy with which the theory could predict the burning rate of composite propellant in an actual rocket motor still remained to be determined by experimental tests however. It was my plan to conduct these tests. In general, results of industrial tests showed that the burning rate of propellant in a rocket motor differed markedly from that of a strand of identical propellant; in most cases the burning rate in a rocket motor was said to be greater than that of a strand, though in some cases the reverse was found for unexplained reasons. It was postulated that a "scale" effect existed between a rocket motor grain and a propellant strand due to the different conditions under which combustion took place in the two cases. The most obvious reason for the existence of this so-called scale effect is the effect on the burning rate of radiant energy feedback to the propellant surface. Other factors yet unknown may contribute to cause this scale effect. It was decided to investigate theoretically and experimentally the magnitude of the radiant flux from the combustion gases incident upon the surface of

burning composite solid propellant, and consequently to test the applicability of the granular diffusion flame theory of composite propellant burning rate to rocket motors.

III. Effect of Radiation on Composite Propellant Burning Rates

The original development of the Summerfield granular diffusion flame theory assumed that radiation was a negligible mode of energy transfer to the burning surface of a composite, solid propellant compared with conduction from the flame zone to the propellant surface. The change in burning rate due to the inclusion of terms corresponding to radiant heat transfer in the granular diffusion flame theory was developed by Professor Summerfield and is reviewed later in this thesis. Results are presented in (2) and in this thesis. The possible sources of radiant energy are the thin reaction zone of the solid propellant flame and, in a rocket motor, the hot combustion gases present in the central grain cavity or "core".

Experimental determination of the radiant energy from the propellant flame was performed by D. W. Blair. (2), (9), (11). A theoretical prediction of the radiant heat transfer from the hot combustion gases to the propellant grain in the experimental rocket motor and an experimental check of the validity of the prediction was my task.

In making these tests it was hoped that a reliable evaluation of the role of radiant energy in solid propellant combustion could be made and consequently reveal the general applicability of the modified Summerfield granular diffusion flame theory for the analytical determination of composite, solid propellant burning rates.

IV. The Strand Burner as a Solid Propellant Research Tool

Use of the granular diffusion flame theory of composite propellant burning rates is dependent upon the accurate determination of the parameters (a) and (b) from measurements made from burning strands. Accurate measurement of these parameters is possible only if the research tool used is capable of producing data having a low scatter. Since, at present, the strand burner is the usual research tool, it was decided to investigate the desirability of using strands for burning rate measurements and to develop the strand burner to a point where the burning rate data obtained had as low a scatter as possible, preferably 1% or less. The data obtained would then be compared with rocket motor burning rate data. This investigation (2, 9) was performed in conjunction with the rocket motor tests. A summary may be found in Appendix IV. The results of this investigation and strand burner development indicated that the random errors associated with measuring the burning rate of a given diameter strand might be kept to a 2% standard deviation or less. Typical results of such testing were obtained by the author from 1/4" diameter strands of propellant identical with the propellant used in rocket motor tests and are shown in Figure 5. The random scatter in these tests was less than 1% standard deviation.

CHAPTER II

BURNING RATE DETERMINATION FROM ROCKET MOTOR EXPERIMENTS WITH RADIAL BURNING GRAINS

I. Grain and Rocket Motor Configuration--Criteria and Design.

In a solid propellant rocket motor the chamber pressure variation with time is related directly to the area of burning surface of the propellant for a fixed nozzle diameter. There are three general classifications of pressure-time relations in a solid propellant rocket motor using any particular grain design and its associated burning surface. These classifications are called progressive, neutral, and regressive burning characteristics and directly indicate the manner in which the area of propellant burning surface varies with time (6). A progressive burning characteristic indicates that the burning area of the propellant increases with time, resulting in a continuous chamber pressure increase. Regressive burning is the converse of progressive burning and indicates that the chamber pressure decreases with time, while a neutral burning characteristic means that the chamber pressure in the rocket motor remains constant with time during the firing. There are combinations of these characteristics due to special grain design but these need not concern us at this time.

Experimentally, it has been found that the burning rate of a solid propellant is a function of the pressure on the burning surface of the propellant. A progressive burning grain was used because it reduced the necessary number of rocket motor test firings by providing data over a range of pressures in a single firing. A cylindrical grain having a cylindrical inside port was chosen. This grain would burn radially outward from the port surface and provide an increasing burning surface and chamber pressure. In theory, the surface of this grain would be a series of concentric cylinders of

constant length. This would make relatively simple the analysis necessary to obtain the burning rate versus pressure curve of the propellant from the test firing.

In the actual design of the radial burning grains to be used in these tests, several related factors had to be considered. These factors were: the weight of propellant that could be formulated at one time, the prevention of erosive burning effects, the chamber pressures obtainable from any ratio, K_N, of burning surface area to nozzle throat area, and the minimum nozzle diameter (to be greater than or equal to 1/4 inch) to prevent nozzle constriction from thermal expansion during firing. Increased burning rates due to gas flow scrubbing of the burning surface--erosive burning--were eliminated by using a ratio of grain port to nozzle throat area greater than or equal to 10. The ratio, K_N, as a function of chamber pressure for a typical propellant used in the Princeton University research on solid propellants was calculated from the equation

$$K_N = \frac{P_c \left[g k \left(2/k-1\right)^{\frac{k-1}{k+1}} \right]^{1/2}}{r\, \rho_p \left[R/MW \times T_g \right]^{1/2}}$$

P_c = pressure, psi

r = burning rate, in/sec

g = acceleration of gravity

k = ratio of combustion gas specific heats, 1.235 (6)

ρ_p = density of solid propellant, 0.0637 #/in^3

R = universal gas constant

T_g = temperature of combustion, assumed to be adiabatic flame temperature, 4260°R

MW = molecular weight of combustion products, 23.45#/mole

P_c and r data for a 75:25, P-13, NH_4ClO_4, propellant were obtained from (5) and the resulting K_N-P_c curve is shown in Figure 6. The weight of propellant that could be formulated at one time was formerly 600 grams. After the motor and grain design was fixed and the necessary equipment constructed, improved propellant formulation procedures enabled me to make twice this amount of propellant at one time.

The first step in designing the necessary grain dimensions was to determine the nozzle throat diameter using the above mentioned four factors. This was done by writing an equation for the weight of the propellant grain in terms of the ratios mentioned in the design factors and solving for the throat diameter.

$$d_t = \sqrt{\frac{16W}{\sqrt{10}\,\rho_p \pi K_{N_1}\left[\left(\frac{K_{N_2}}{K_{N_1}}\right)^2 - 1\right]}} \qquad (2)$$

W = weight of propellant, #

d_t = throat diameter, in.

ρ_p = density of propellant

K_{N_1} = value of K_N at start of combustion

K_{N_2} = value of K_N at end of combustion

A derivation of this relation is given in Appendix I. The port diameter, grain length, and outside grain diameter were then determined by the equations:

$$d_p = \sqrt{10}\, d_t \qquad (3)$$

$$L = \frac{d_t K_{N_1}}{4\sqrt{10}} \qquad (4)$$

$$D = \frac{d_p K_{N_2}}{K_{N_1}} \qquad (5)$$

where

d_p = port diameter, in

L = grain length, in

D = outside grain diameter, in

From Figure 6, the values of K_N were found for the desired change in chamber pressure during the motor test. The corresponding grain dimensions and nozzle throat diameter were calculated via Equations (2) through (5). The grain dimensions arrived at by the preceding method of calculation did not include the increase in grain size due to the necessity of inhibiting the grain to prevent combustion from taking place anywhere but on the grain port surface. A 1/8" thickness of inhibitor was deemed necessary to prevent the initiation of combustion on any surfaces. At the time that this consideration was brought to light, the grain molds and combustion chamber had already been constructed and the maximum inhibitor thickness on the low pressure grain could be only 1/16 inch. It was later found this thickness was satisfactory even at pressures as high as 1000 psi. The medium and high chamber pressure grains were smaller in diameter and readily permitted a 1/8" inhibitor thickness. In fact, it was decided to use enough inhibitor on the outside cylindrical portion of the grains to make their maximum diameter correspond to the inside diameter of the rocket combustion chamber. This eliminated the necessity of providing a mechanical support for each grain to hold it in the center of the combustion chamber (Figures 12, 13).

Having fixed grain dimensions and their associated nozzle diameters, the physical design of the nozzles and combustion chamber was accomplished.

Since it was unnecessary to measure the thrust level of the rocket motor to determine the propellant burning rate, a simple converging, choked nozzle design was used for each range of chamber pressures. The nozzles were made interchangeable by designing them to be slipped into the nozzle holder plate at the rear end of the motor, see Figure 7. A metal-to-metal seal between the shoulder of the nozzle block and the nozzle holder plate, utilizing the motor chamber pressure to provide the sealing force, prevented the combustion products from escaping anywhere but out the nozzle, Figure 10. The nozzle converged at a 30° angle to the throat with a 0.5 inch radius at the transition to the throat diameter. Copper was used, because of its high thermal conductivity, in the nozzle block to prevent nozzle burnout, and a molybdenum insert in the throat section prevented nozzle erosion by the hot, high velocity rocket exhaust. Molybdenum was selected for the nozzle insert material because of its relatively high heat conductivity and lack of chemical reaction in the reducing atmosphere of the rocket exhaust. No measurable erosion or change in nozzle diameter was noted in the process of rocket motor testing. Later, an all copper nozzle was employed for some motor tests without any measurable erosion, raising the question of the necessity of using a molybdenum insert in future, short run duration, motor tests.

It was decided to use one combustion chamber size for all grains to be fired, and the maximum grain length and diameter fixed this size. A spacer between the front wall of the combustion chamber and the grain was used in each case to supply a stagnant pocket of gas at the pressure tap and leave room for igniter placement. The chamber wall was designed to burst at 4000 psig to minimize explosion hazard in case of a motor malfunction, and a burst

disc assembly--disc burst pressure was 3000 psig-- see Figure 8, was employed. To facilitate grain loading and nozzle changing, the nozzle holder plate was designed to screw into the combustion chamber and a gas seal was effected by a spiral wound, metal-asbestos gasket compressed between the nozzle holder plate and the combustion chamber. The motor mount was simply a section of I-beam bolted to the test stand's concrete floor with a simple A-frame to hold the motor itself.

II. Final Rocket Motor, Nozzle and Grain Dimensions

The final rocket motor, nozzle, and grain dimensions are given in Table I, Appendix I; more details of the rocket motor are given in Figure 10.

III. Grain Preparation

The propellant formulation used in making solid propellant grains was a standard type used in previous Princeton University research. The basic constituents were ammonium perchlorate crystals for the oxidizer and a styrene based, polyester resin as the fuel. The oxidizer was obtained from American Potash and Chemical Company designated "Aerojet As Received." The fuel resin was obtained from Rohm & Haas Company and had the designation "P-13." The composition of the propellant is given in Table I with the numbers indicating percent of the total amount. This propellant formulation was densely loaded with oxidizer and consequently provided combustion conditions closer to stoichiometric than any other Princeton formulation. This resulted in increased combustion efficiency but also a faster burning rate than a less oxidized propellant. The increased burning rate meant short firing times in the rocket motor with only a small increase in the adiabatic flame temperature. Thus the heat loss to the rocket motor's metal

components was less than that loss would have been with a slower burning propellant. It was felt that the decreased firing time would not adversely affect the accuracy of the data obtained from the chamber pressure versus time trace recorded during each motor test. Furthermore, the very viscous nature of this propellant made it easy to fill the grain molds and insert the mandrels without excess propellant from the mold being lost through spillage.

TABLE I

Rocket Motor Solid Propellant Composition
Designated AP 80:20, Princeton University

P - 13		19.75
Nuodex Cobalt		0.1
Lecithin		0.1
NH_4ClO_4		
Unground	56.0	
Ground	24.0	
Total Oxidizer		80.0
Methyl Ethyl Ketone Peroxide (MEKP)		0.05
Total		100.0

IV. Pressure Recording Systems

Two methods of obtaining and recording the chamber pressure-time history of the rocket motor during a test were used, both being tested concurrently to ascertain the best method. The first method utilized a miniature slide-wire potentiometer type pressure transducer. The transducer output was fed into an oscilloscope set for a sweep rate of one centimeter per second and a photograph taken of the resulting pressure trace. The transducer was mounted on the floor of the test cell to eliminate noise signal due to vibration during firing. The second method used a bourdon tube sensing element whose deflection was recorded on a chart recorder. The complete instrument was made by the Esterline-Angus Company. In both cases, the pressure sensing elements were protected by having the pressure impulse transmitted to them by hydraulic fluid in a line from the element to the rocket motor chamber. In the case of the Esterline-Angus recorder, the line was of a much greater length and was fitted with a needle valve to act as a snubber for most of the high frequency, high pressure impulses when the igniter went off. It was decided that the Esterline-Angus recorder was the best as it produced a physically larger data image, making it easier to reduce the errors involved in calculating the instantaneous burning rate. In addition, since the electric pressure transducer had a range from 0-3000 psig, the high oscilloscope sensitivity necessary to get a useful trace at low maximum chamber pressures revealed the integral step in the output of the transducer when the sliding contact changed from coil to coil. This type of output made it impossible to get continuous chamber pressure versus time data. The only disadvantage in using the Esterline-Angus recorder was that the data had to be replotted on rectilinear paper before the pressure-time trace could be used to obtain burning rate data. This replotting could be done to an accuracy of about $\pm$ 5 psi from the Esterline-Angus record chart, which was within the $\pm$ 10 psi accuracy available from the recorder itself. Due to the presence of a pressure pulse

snubber in the pressure pickup line to the recorder, the response time was known only to be of the order of 1/4 to 1/2 a second. For the purpose of analysis, the start of steady-state burning was assumed to be when the extrapolated pressure curve made an intersection with a line perpendicular to the time axis, drawn from the time of igniter discharge. Although this caused a slight error in mass consumption computations because the chamber pressure build-up time was neglected, the mass fraction so assumed was very small compared to the total propellant mass available.

V. Initial Test Results

Initial test results were quite disappointing since the pressure-time trace obtained showed a rather slow tail off--or cessation of chamber pressure and hence burning--rather than the sharp cut-off expected from a uniformly, radial burning grain. Several explanations arose--non-uniform ignition of the port surface, propellant voids, cracking of the grain due to a high pressure impulse from the igniter, uneven ignition due to the inbedding of hot igniter particles deeply into the propellant because the igniter had been placed in the port of the grain. It was decided that an investigation of the propellant burning surface should be made by quenching the grain during a motor test. Consequently a water quenching system was set up, see Figure 15.

The possibility of propellant voids causing a non-radial burning surface was investigated by forming some grains of a 75:25 composition, which was very soupy in the uncured state and easily deaerated during the grain molding process. These grains exhibited the same long cut-off period originally found in the 80:20 grain formulation. This indicated that propellant voids formed during the grain formulation process were not the cause of the long cut-off period (herein referred to as "tail-off.")

Water quenching of both 75:25 and 80:20 propellant grains with the igniter placed in the grain port showed that there were indeed holes in the radial burning surface, varying in diameter from about one-half inch to one-and-one-half inches, but no evidence of grain cracking was seen. It was concluded that hot particles of the igniter were imbedding themselves in the propellant surface upon igniter firing and causing local holes to be formed, Figure 16.

At this point the igniter must be described. It was of the "jelly roll" type consisting of magnesium powder mixed in a slurry, spread evenly thick on a cellophane back, and allowed to dry. The subsequent sheet was cut into strips and rolled around an electrical squib. It could be made in any desired weight. We used a 6gm jelly roll, made by Special Devices, Incorporated which had an ignition time to ignite all the magnesium powder of approximately 20 milliseconds. It was decided to obtain a "slow acting" 6gm jelly roll and at the same time develop an igniter using hot gases to ignite the propellant. The hot gas igniters used an electric match igniting a BBC blackpowder and scrapings of solid propellant. These igniters were found to produce poorly repeatable ignition results. With the arrival and testing of the slow acting jelly roll igniters, the hot gas igniters were abandoned.

Quench tests of grains, ignited with the slow acting jelly roll were made. The igniters were anchored in the spacer so that the burning magnesium particles were swept past the scraped surface of the grain port. The quench tests showed that there was no pitting of the propellant and uniform, radial burning. The ignition problem was then considered to be solved.

As indicated above, the water quenching of burning grains was very successful in the interruption and extinguishing of the burning grains. The method used incorporated a spray rake. This spray rake was inserted in the

front end of the rocket motor on its centerline and projected a heavy, radial spray of water on the grain port surface in the combustion chamber, Figure 18. A water flow rate of approximately fifty gallons per minute immediately quenched the burning, as indicated by the pressure-time trace of a quenched grain in Figure 17.

Examination of several quenched grains, burning at low and high chamber pressures, revealed an interesting, general characteristic of the burning surface, Figure 18. A sketch of a typical, quenched grain surface is shown below and

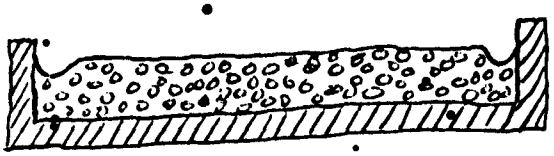

may be interpreted in terms of the properties of cast propellant learned from the studies conducted by D. W. Blair on strands. The small dip--exaggerated in the sketch but uniform all around the grain--in the propellant surface is explained by the tendency of propellant to burn faster near a molded surface. A "molded surface" is that portion of a casting of solid propellant which was in contact with the surface of the casting mold. The reason for the small rise in the surface level; immediately adjacent to the inhibitor, may be explained by the complete removal of oxidizer crystals at the grain surface during the removal of the mold release agent associated with the preparation of the cured grain for inhibiting. The lack of oxidizer immediately next to the grain surface would cause a slowing of the burning rate at this surface. The increase in area due to the dips was small and it was concluded that for the purpose of data reduction, radial burning took place until the dips reached the outside inhibitor surface. At this point, the burning surface area started to decrease as the edges of the dip

burned toward the center of the grain. The resulting decrease in surface area, once the dips reached the outside inhibitor surface, caused the chamber pressure to decrease as the remaining propellant was consumed and formed the observed "tail-off". The final conclusion concerning data reduction was that the burning rates could be calculated safely up to the point of maximum chamber pressure, assuming that the burning was uniformly radial. The area increase due to the dips was less than 3%.

The initial testing also revealed that the calculated K_N data used in the original design of the grain and nozzle diameter was low. That is, ratios of K_N greater than calculated were necessary to obtain the desired pressure variations. To see this, see the curves on Figure 6. Subsequent experimental K_N values of 80:20 propellant were determined and it was found that the use of two new, smaller diameter nozzles--of 0.359 inch and 0.250 inch diameter, respectively--and the low and medium pressure grain designs would produce the desired range in pressure variation from 200 psig to 1500 psig, inclusive.

Calculation of burning rates at low chamber pressures revealed approximately 15% lower burning rates than those determined from strands. It was decided to go to higher maximum chamber pressures and determine the associated burning rates to see if the trend continued. This was done using the new, smaller nozzles and the low and medium pressure grain designs.

VI. Data Reduction Procedure

As mentioned previously, one of the advantages in using a radial burning grain was the relative ease of calculating the propellant burning rate from the pressure-time curve recorded during the motor test. The procedure for these burning rate calculations was to equate the propellant mass

consumed by combustion to the mass outflow through the nozzle. A term involving the rate of gas mass increase inside the combustion chamber was very small compared to the other terms and was discarded in the burning rate analysis. The mass of propellant consumed is directly proportional to the difference in grain port radius squared at a given time and the initial port radius squared. Hence an expression for the instantaneous radius as a function of time, instantaneous chamber pressure, the integrated area under the pressure-time curve up to that time, and the characteristic velocity c* could be obtained. The time derivative of this expression is the instantaneous burning rate of the propellant. For a complete derivation of the expression determining the burning rate, and an example of the data reduction procedure, see Appendix II. This method of data reduction is similar to that given in (8).

The pressure-time trace obtained directly from the Esterline-Angus recorder was not a rectilinear plot since the recorder pen, actuated by the bourdon tube pressure sensing element, traced an arc on the recorder paper, Figure 19. Therefore, it was necessary to replot the recorded data on rectilinear coordinate paper since area is not conserved under transformation of one coordinate in a two coordinate system. This was done in all cases and a typical pressure-time trace, replotted on rectilinear paper, is shown in Figure 20.

Originally, the integration of the area under the replotted pressure-time curve for each run was done with a planimeter. This process was very time consuming and it was found that the method of trapezoids was much faster and just as accurate as a planimeter. A method of integration using Simpson's Rule was also tried but the smallest convenient division of the time scale into equal elements of time did not give as good accuracy as the above two methods, and the method was discarded.

The average c* for each test firing was found by dividing the entire, integrated area under the pressure-time curve by the weight of propellant and inhibitor burned.

$$c^*_{exp.} = A_t g \int_0^{t_f} P_c dt / W'$$

A_t = nozzle throat area

$c^*_{exp.}$ = experimental characteristic velocity

t_{final} = total combustion time

P_c = instantaneous chamber pressure

W' = weight of propellant and inhibitor burned

g = acceleration of gravity

The experimentally determined c*'s showed a variation from 4,300 ft/sec. to 4,710 ft/sec. In the tests reported in this thesis. It was decided to use an average, experimental c* of 4,520 ft/sec. for the data reduction to obtain burning rates. The percentage deviations of experimental c*'s from this average c* are approximately $\pm 5\%$. The total weight of propellant and inhibitor burned was used for these c* determinations because a small quantity of the inhibitor was burned by the hot combustion gases and subsequently exhausted out the nozzle. The weight of inhibitor burned contributed to the chamber pressure and mass flow out the nozzle of the rocket motor and therefore had to be included in the calculation of the experimental c*. W' was determined by weighing the inhibited grain before firing and weighing the inhibitor after firing, the difference being the weight of combustion gases which flowed out the rocket nozzle.

The use of only one value of c*, 4,520 ft/sec., instead of an instantaneous c* for each pressure in the calculation of the burning rate as a function of pressure resulted in a decrease of data point scatter of the burning rate vs. pressure curve.

VII. Final Results of Motor Tests and Comparison with Strands

The calculated burning rates as a function of chamber pressure from the rocket motor tests are shown in Figure 21. These tests gave the unexpected result that the average burning rate of the propellant in the rocket motor was lower by 3 to 13% than the rate determined from extruded strands of identical propellant. It must be noted that the discrepancy decreased as the chamber pressure increased, though no reason for this is available at present. At first it was thought that the heat loss and consequent decrease in c* at relatively low chamber pressures (around 300-500 psi) was responsible for the 10% discrepancy. However a short calculation, assuming an upper limit of heat loss, resulted in an approximate decrease in burning rate of only 1.5% and did not explain the 10% discrepancy observed. Later error calculations (Appendix II) show that the discrepancy is partially due to the uncertainty of the correct value of c* used in the burning rate calculations.

The investigations of Blair (2), (9) showed that extruded strands tend to burn about 7% faster than strands having no mold surfaces. Since the rocket motor test grains had very little molded surface, it was to be expected that a low value of burning rate be found. However, the effect of the adiabaticity with respect to radiation, of a radial burning grain, was expected to cause the grain to burn approximately 11% faster than a strand of the identical propellant having no molded surfaces. This did not appear to be the case. In view of these test results it was decided to inspect closely the role of radiation in solid propellant combustion, both in a strand and in a radial burning grain.

CHAPTER III

EFFECT OF RADIATION ON THE BURNING RATE OF SOLID PROPELLANT IN STRANDS AND MOTORS

I. Theoretical Analysis Showing Δr Due To Radiation

The original derivation of the Summerfield Granular Diffusion Flame expression for composite propellants, (2) and (10), considered that conduction was the only mechanism feeding energy to the propellant surface from the reaction zone. Recently a radiation component has been added to account for possible radiative energy feedback. The results of this addition, referring to the following sketch and using the following symbols is given below. (This analysis may be compared with the results in (2).)

I_F = radiant energy flux feedback from flame

I_L = radiant energy flux loss from flame

I_x = radiant energy flux into flame zone from external sources (e.g., I_{core} from a hot gas core in a hollow burning grain)

α_F = Fraction I_x absorbed before the solid surface

Q_c = enthalpy of combustion $c_{pg}\,(T_{1(ad)} - To)$

T_{1f} = final temperature of combustion products

$T_{1(ad)}$ = final temperature (adiabatic case)

T_s = temperature of solid surface--assumed independent of P, valid if $E_{act} > 2$ kcal/mole

T_o = ambient propellant temperature

r_o = hypothetical burning rate in absence of radiation

r = actual burning rate with radiation term included

ρ_p = density of solid propellant

C_s = specific heat of solid propellant

Q_s = exothermic heat of solid to gas reaction at surface

C_{P_g} = specific heat of combustion products

τ_o = adiabatic gaseous reaction time in flame

τ = actual time for gaseous reaction

For the general case including all types of radiative energy loss and gain, the change in propellant burning rate may be derived as follows. With reference to the sketch below, the energy equation for a burning strand may be written as

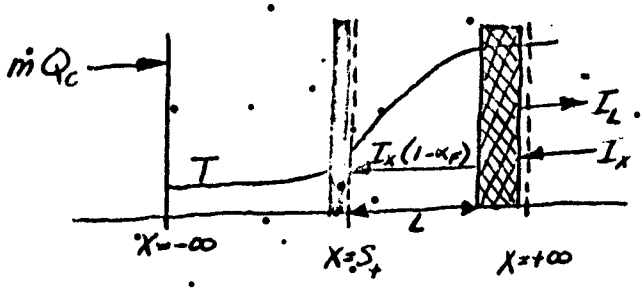

$$\underbrace{\dot{m}Q_c}_{x=-\infty} = \underbrace{\dot{m}C_s(T_s-T_o) - \lambda_{gs}\left(\frac{\partial T}{\partial x}\right)_{gs} - I_F + \dot{m}(Q_c-Q_s) - I_x(1-\alpha_F)}_{x=S_+} \qquad (1)$$

$$\underbrace{\dot{m}Q_c}_{x=-\infty} = \underbrace{\dot{m}C_g(T_1-T_o) + I_L - I_x}_{x=+\infty} \qquad (2)$$

From Equation 2, determine T_1

$$T_1 = \frac{1}{\dot{m}C_g}\left[\dot{m}C_gT_o + \dot{m}Q_c + I_L - I_x\right] = \frac{1}{\dot{m}C_g}\left[\dot{m}C_gT_{1(ad)} + I_x - I_L\right] \qquad (3)$$

since $\dot{m}Q_c = \dot{m}C_g(T_{f(ad)} - T_0)$. Now solve for $\left(\frac{\partial T}{\partial x}\right)_{g_s}$ in Equation 1:

$$\left(\frac{\partial T}{\partial x}\right)_{g_s} \cong \frac{T_f - T_s}{L} = \frac{1}{L}\left(T_{f(ad)} + \frac{I_x}{\dot{m}C_g} - \frac{I_L}{\dot{m}C_g} - T_s\right) \tag{4}$$

where L is the distance between the surface of the propellant and the flame front. Estimation of the value of L may be done by assuming that the density of gas between the surface and the flame front per unit of surface area is a function only of the distance between the propellant surface and the flame front. It is also argued that this distance is increased due to incident radiation on the propellant surface since less energy feedback by conduction is necessary to vaporize the surface propellant. We may then write that

$$L_R \cong \frac{\dot{m}}{\rho_g} \cong L_0 \cdot \frac{\dot{m}}{\dot{m}_0} \cdot \frac{\tau}{\tau_0} \tag{5}$$

where the zero subscript denotes no radiation, adiabatic flame condition. Substituting for $\left(\frac{\partial T}{\partial x}\right)_{g_s}$ expressed in terms of T_f and L_R into the energy equation we obtain

$$0 = \dot{m}\left[C_s(T_s - T_0) - Q_s\right] - \left[I_F + (1-\alpha_F)I_x\right] - \lambda_{g_s}\left[\left(T_{f(ad)} - T_s\right) + \frac{I_x - I_L}{\dot{m}C_g}\right]\frac{1}{L_0 \cdot \frac{\dot{m}}{\dot{m}_0} \cdot \frac{\tau}{\tau_0}} \tag{6}$$

It has been assumed that T_s is approximately constant. This is true for large values of activation energies and may be seen from an examination of the mass flow rate with respect to the pyrolysis rate of the propellant.

$$\dot{m} = \rho_p r_{Pyrolysis} = \rho_p A \exp\left(-\frac{E_{activation}}{R T_s}\right)$$

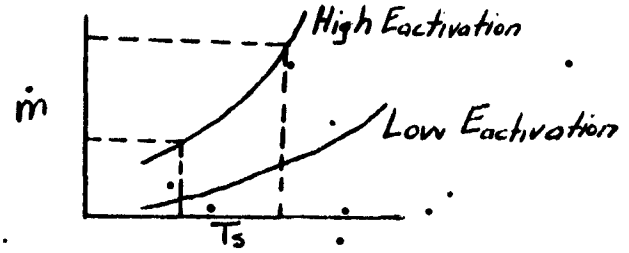

Since $\dot{m}$ is constant at a constant pressure, the above sketch shows that for a large activation energy, the surface temperature, T_s stays constant.

Noting that

$$\frac{\lambda_{gs}(T_{1(ad)} - T_s)}{L_o} = \dot{m}_o\left[C_s(T_s - T_o) - Q_s\right] \tag{7}$$

a four term equation, cubic in $\dot{m}$, may be written from Equations (6) and (7) with no further assumptions as:

$$\dot{m}^3\left[C_s(T_s - T_o) - Q_s\right] - \left[I_F + (1-\alpha_F)I_F\right]\dot{m}^2 - \dot{m}_o^2\left[C_s(T_s - T_o) - Q_s\right]\left(\frac{\tau}{\tau_o}\right)\dot{m}$$

$$+ \dot{m}_o^2 \frac{(I_x - I_L)\left[C_s(T_s - T_o) - Q_s\right]}{C_g\left[T_{1(ad)} - T_o\right]}\left(\frac{\tau}{\tau_o}\right) = 0 \tag{8}$$

To solve for $(\dot{m}/\dot{m}_o)$, assume $\left|\frac{\dot{m}}{\dot{m}_o} - 1\right| << 1$. Divide Equation (8) by $\dot{m}_o^3\left[C_s(T_s - T_o) - Q_s\right]$ and let $(\dot{m}/\dot{m}_o) = 1 + \delta$ and retain only those terms of order δ^0 and δ^1. Then $\left[I_F + (1-\alpha_F)I_x\right]/\dot{m}_o\left[C_s(T_s - T_o) - Q_s\right]$ and $(I_x - I_L)/\dot{m}_o C_g(T_1 - T_s)$ terms are of order δ and the resulting equation is:

$$0 = (1+3\delta) - \frac{\left[I_F + (1-\alpha_F)I_x\right]}{\dot{m}_o\left[C_s(T_s - T_o) - Q_s\right]} - \frac{\tau_o}{\tau}(1+\delta) - \frac{\tau_o}{\tau}\frac{(I_x - I_L)}{\dot{m}_o C_g(T_{1(ad)} - T_o)} \tag{9}$$

Now note that (τ_o/τ) is order of $(1+\delta)$; then

$$(\tau_o/\tau)(1+\delta) \longrightarrow (\frac{\tau_o}{\tau}+\delta)$$

and $\frac{\tau_o}{\tau}\frac{(I_R - I_L)}{\dot{m}_o C_g(T_{1(ad)}-T_s)} \longrightarrow \frac{(I_R-I_L)}{\dot{m}_o C_g(T_{1(ad)}-T_s)}$. Using the

above relationships in Equation (9) we obtain:

$$0 = 2\delta - \frac{[I_F + (1-\alpha_F)I_R]}{\dot{m}_o[C_s(T_s-T_o)-Q_s]} - (\frac{\tau_o}{\tau}-1) - \frac{(I_R - I_L)}{\dot{m}_o C_g(T_{1(ad)}-T_s)}$$

and

$$\left(\frac{\dot{m}}{\dot{m}_o}-1\right) = \frac{\frac{1}{2}[I_F+(1-\alpha_F)I_R]}{\dot{m}_o[C_s(T_s-T_o)-Q_s]} + \frac{\frac{1}{2}(I_R-I_L)}{\dot{m}_o C_g(T_{1(ad)}-T_s)} + \frac{1}{2}\left(\frac{\tau_o}{\tau}-1\right) \qquad (10)$$

Putting Equation (10) in terms of burning rates, the general equation for the change in burning rate due to radiation, Δr_1 divided by the burning rate with no radiation is

$$\frac{\Delta r}{r_o} = \frac{\frac{1}{2}[I_F+(1-\alpha_F)I_R]}{r_o\rho_p[C_s(T_s-T_o)-Q_s]} + \frac{\frac{1}{2}(I_R-I_L)}{r_o\rho_p C_g(T_{1(ad)}-T_s)} + \frac{1}{2}\left(\frac{\tau_o}{\tau}-1\right) \qquad (11)$$

We are now able to investigate the effect of radiation in propellant burning rates in strands and motors (2), For the case of the burning strand where

$I_R = 0$, $I_L = I_F$, $T_1 < T_{1(ad)}$ and $\tau_o/\tau < 1$, Equation (11) becomes:

$$\frac{\Delta r}{r_o} = \frac{\frac{1}{2}I_F}{r_o\rho_p[C_s(T_s-T_o)-Q_s]} - \frac{\frac{1}{2}I_R}{r_o\rho_p C_g(T_{1(ad)}-T_s)} + \frac{1}{2}\left(\frac{\tau_o}{\tau}-1\right) \qquad (12)$$

In the case of a hollow grain, burning on the inside surface, $I_R < I_{core} + I_L$, $I_L = I_F$, $\alpha_F << 1$, $T_1 = T_{1(ad)}$ and $\tau_o/\tau = 1$ are assumed. Then

$$\frac{\Delta r}{r_o} = \frac{I_F}{r_o\rho_p[C_s(T_s-T_o)-Q_s]} + \frac{\frac{1}{2}I_{core}}{r_o\rho_p}\left\{\frac{1}{[C_s(T_s-T_o)-Q_s]} + \frac{1}{[C_g(T_{1(ad)}-T_s)]}\right\} \qquad (13)$$

II. Investigation of Flame Zone Radiation and Results

The investigation of the flame zone radiation was undertaken by D. W. Blair, (2), (11), and was accomplished by means of a strand burner equipped with an optical window and a series of apertures shown in Figure 28. Values of I_L where observed for various propellants at a range of pressures. Measurements of I_L from flames of strands (80:20 mixture), burning at 500 psig came out to be 6.4 cal/cm^{2}sec or a flame emissivity of 0.075 based on a theoretical flame temperature of 2800°K.. Insertion of this I_L into Equation (12) assuming $I_F = I_L$ gives

$$\frac{\Delta r}{r_o} = 0.020 - 0.006 + \frac{1}{2}(0.93 - 1) = -0.021 \qquad (14)$$

This result means that the burning rate of a strand predicted by the granular diffusion flame theory when the effects of radiation are included, is less than the burning rate predicted by the equation $\frac{1}{r_o} = \frac{a}{P} + \frac{b}{P^{1/3}}$ which neglects radiation, by approximately 2%. The effect of radiation is indeed small, but is not negligible in the prediction of propellant burning rates.

III. Theoretical Investigation of Radiant Energy Feedback in a Rocket Motor

An investigation of the radiant heat feedback to the burning surface of a radial burning grain in a rocket motor, due to the radiation of the hot combustion gases, was initiated. Previous research at Princeton gave the approximate mole fractions of significantly radiating combustion products for an 80:20, P-13 propellant as:

Component	Mole Fraction
CO_2	0.0591
H_2O	0.244
CO	0.319
HCl	0.151

The shape of the radiating gas column was assumed to be a cylinder and the approximate optical path length was computed, from (16), to be 0.2 feet for the radiation impinging on the cylindrical surface of the burning propellant grain. Detailed calculation of the radiant heat feedback is given in Appendix III.

The emissivities of the water vapor and carbon dioxide present in the combustion gas were computed, from (14) to be 0.182 and 0.0552 respectively, for a total pressure of 500 psi and a temperature of 2800°K. Since both CO_2 and H_2O were present it was necessary to account for their mutual absorption and determine a combined emissivity for CO_2 and H_2O as 0.1472.

Emissivities for CO and HCl molecules were calculated using the following equation from (12):

$$\epsilon = \left[1 - \exp(-k_F P_i L_e)\right]\epsilon_F + \left[1 - \exp(-k_{FO} P_i L_e)\right]\epsilon_{FO} \qquad (15)$$

k_F = average absorption coefficient of fundamental vibration-rotation band for i^{th} component

K_{FO} = average absorption coefficient of first overtone vibration-rotation band for i^{th} component

ϵ_F = emissivity of fundamental vibration-rotation band

ϵ_{FO} = emissivity of first overtone vibration-rotation band

P_i = partial pressure of i^{th} component

L_e = optical path length

Equation (17) gave the emissivity of CO and HCl at 500 psi and 2800°K as 0.0304 and 0.0318, respectively, for radiation to the grain's burning surface.

The total emissivity of the hot combustion gases at 500 psi and 2800°K was then found to be $\epsilon_T = 0.145$ giving a radiant heat feedback

to the grain surface, according to equation $q = \epsilon \sigma T^4$, of 12.2 cal/cm^{2}sec. This heat flux is approximatly twice the flux to the flame zone as determined by Blair.

IV. Experimental Measurement of Radiant Energy of Combustion Products in Rocket Motor

Since the preceding calculations showed that radiant energy feedback to the grain surface from the combustion gases was appreciable, it was decided to check the calculation by experiment.

The rocket's combustion chamber was modified to include a window on its longitudinal axis, looking through the rocket nozzle. An aperture system was designed so that a radiation thermocouple (Model RP-2, Charles Reeder Co., KBr optics) could "see" through the combustion gases in the rocket chamber and out through the rocket's nozzle. The radiation thermocouple was exposed to radiation from the combustion gases only, and none from the hot metal components of the rocket engine. A small N_2 purge was constructed to keep the window in the rocket motor clean during a motor firing. A schematic of the experimental equipment just described is shown in Figure 24.

The output from the radiation thermocouple was amplified by a Kintel differential amplifier and sent to an oscilloscope where the signal was photographed. Since the output of the radiation thermocouple is due to the difference in temperature between the senstive element and the thermocouple case, it was necessary to reduce the test cell temperature to the outside, ambient temperature to minimize the effect of convection currents in the test cell during the motor test. The case of the thermocouple was also insulated to help stabilize the case temperature.

One test was made using quartz optics and three tests were

made with KBr optics to allow radiation in the far infrared to be recorded. Alignment of the thermocouple with the aperture system was accomplished by placing a 100 watt titanium filament lamp at the rocket nozzle and placing the thermocouple in the center of the resulting beam of light through the aperture system. The thermocouple receiver was isolated from vibration during a motor test to maintain alignment with the aperture system.

A typical radiation trace obtained from a motor test is shown in Figure 24. The large peak at motor ignition is due to radiation of the burning magnesium from the jelly roll igniter. The peak just before the completion of burning is due to the relatively large amount of glowing soot from the burning inhibitor at this point in the test. Radiant energy measurements obtained from the one test using quartz optics were approximately twice the value of radiation measurements obtained using KBr optics. Since the three tests using KBr optics correlate quite closely, it is postulated that the aperture system, in the quartz optics test, was not properly aligned and the radiation thermocouple "saw" a part of the rocket nozzle, which would have a much higher emissive power than the combustion products.

If the results of the three radiation tests using KBr optics are averaged, the radiant flux received by the radiation thermocouple at a chamber pressure of approximately 500 psi is 275 microwatts/cm^2, or 1.05 watts per steradian subtended by the sensitive area of the thermocouple.

A theoretical prediction of the radiant energy received by an elemental area placed in the same position as the radiation thermocouple was then made, and the analysis is given Appendix III. The extreme rays of the aperture system define a small, circular area, at the base of the hot gas column in the combustion chamber, which is "seen" by the radiation

thermocouple. The sensitive area of the radiation thermocouple was rectangular in shape, 0.2mmX2mm, approximately. It can be shown geometrically, that the circular area formed by the extreme rays of the aperture system intersecting the base of the hot gas column, assuming the thermocouple sensing area to be a point, is very nearly identical with the elliptical area formed by considering the rectangular thermocouple sensing area. This circular diameter was 0.23 cm and was 61.8 cm from the radiation receiver. Since the normal intensity at the center of the 0.23cm circle, at the base of the cylindrical gas column, cannot be differentiated from the normal intensity of a hemisphere whose radius is equal to the length of the hot gas column, the normal intensity of this hemisphere was determined. This intensity was used to predict the radiant energy received at the radiation receiver using the method outlined for radiant energy transfer between elemental areas in references (14) and (16). The radiant energy flux at the radiation receiver was calculated to be 1.49 watts per steradian subtended by the receiver area. The predicted radiant flux is high since no data was available for emissivity corrections due to self absorption in a gas mixture containing CO and HCl as well as CO_2 and H_2O vapor. However, the predicted radiant flux was of the same order of magnitude as the measured radiant flux, leading to the conclusion that the method employed to determine the emissivity of the combustion products is quite accurate. It may be concluded that the calculation, determining the radiant energy flux to the burning surface of the solid propellant grain, is at least of the correct order of magnitude. Therefore the effect of radiation from the combustion gases is of significant importance in determining the propellant burning rate in a rocket motor because it is a significant mode of heat transfer.

As previously mentioned, the theoretical prediction of radiation from the combustion gases to the burning surface of the radial burning grain used in these tests was 12.2 cal/cm^{2}sec. Using a value of I_F = 6.4 cal/cm^{2}sec and the calculated value of I_{core} = 12.2 cal/cm^{2}sec, the $\Delta r/r_o$ due to radiation may be calculated from Equation 13 as

$$r/r_o = 0.040 + (0.0381 + 0.00762) = 0.0857$$

The net effect of flame and combustion gas radiation is seen to be an increase of approximately 11% in the burning rate of the solid propellant in the test rocket motor over the burning rate of a strand. This is apart from erosive effects, strand diameter effects, and mold surface effects.

CHAPTER IV

FINAL STATEMENT ON EXPERIMENTAL COMPARISON OF BURNING RATE OF SOLID PROPELLANT IN STRANDS AND ROCKET MOTORS

I. Summary of Predicted and Experimentally Determined Results

Theoretical considerations led to the conclusion that the burning rate of a solid propellant grain in a rocket motor would exceed the burning rate of a strand of identical propellant by the amount shown by equation 13. Use of equations 12 and 13 coupled with experimental values of I_F and theoretical calculation of I_{core} showed that the burning rate of the solid propellant grain should exceed that of a strand of identical propellant by approximately 11%. This is apart from erosive, strand diameter, and mold surface effects.

Experimental results from motor tests did not show the expected increased burning rates, Figure (21). The rocket motor burning rates averaged from 13 to 2.5% lower than strand burning rates. The fact that extruded 1/4-inch strands were used, means that the experimental curve might be corrected for diameter and mold surface effects. One quarter inch strands tend to burn about 3% slower than 7/16 inch strands, while extruded strands tend to burn about 7% faster than strands with no mold surfaces. The net effect is that the strand burning rate curve shown in Figures (5) and (21) should be lowered by approximately 4%. However, this is not enough to cause the rocket motor burning rate curves to show their expected 11% faster burning rate. The above mentioned 4% correction in strand burning rates in Figure 23 would make the average motor burning rate 1.0% faster than the burning rate in strands at 900 psi.

The motor burning rates were not observed to be 11% faster than

the strand burning rates. Therefore an investigation of the possible error in these motor burning rates is desirable.

II. Errors Involved in the Calculation of the Motor Burning Rate

Examination of the plot of calculated burning rates versus pressure Figure (24) reveals a nonuniformity in the curves. The nonuniformity may be interpreted as being caused by a variation in the constant of integration used in the integral method of obtaining burning rates from the pressure time test data. The constant of integration is the initial radius of the burning surface just after complete ignition. This variation would account for the variation observed in the pressure time traces and could be due to the nonreproducible ignition from the jellyroll igniters. The integral method of obtaining motor burning rates averages the previous history of the burning rate up to the point of the calculation.

The first error analysis in Appendix II shows that the burning rates calculated at 900 psi have approximately $\pm 6.7\%$ error based on the standard deviation of the calculation for any test.

Any calculation from a motor test gives an r versus P curve that is $\pm 6.7\%$ accurate and the variation of the calculated burning rate curves from their average at 900 psi is $\pm 5\%$. Therefore the total possible uncertainty in the results calculated from all the tests is $\pm 11.7\%$. The strand burning rates are included within this error envelope. Therefore results of comparison of strand and motor burning rates are inconclusive.

A second independent check of the uncertainty in the calculated motor burning rates is desirable and should involve the nonuniformity of the pressure time test data. A good measure of the nonuniformity of the pressure time curves is the slope, $\left(\frac{dP}{dt}\right)$. The slope, $\left(\frac{dP}{dt}\right)$, is measured, from each test, at a constant, chosen pressure. A fundamental assumption in

this whole investigation is that the propellant is reproducible because r is regarded as a property of the propellant. If this is not true, then the apparent variation in r from test to test will be due to the variation in propellant as well as any error due to the instrumentation. There is no effect of area in this error measurement because the factor involving area cancels out when finding the value of $\frac{\Delta r}{r}$. The second error analysis in Appendix II shows that at a particular pressure the percentage variation in the instantaneous burning rates from test to test is:

$$\frac{\Delta r}{r} = \frac{\Delta\left(\frac{dP}{dt}\right)}{\left(\frac{dP}{dt}\right)}$$

At 900 psi, the percentage variation, from test to test, of instantaneous burning rate is found to be approximately ±15%, very close to the previously calculated value of the possible error in burning rate calculations.

The conclusion to be drawn from this error investigation is that the present calculations of motor burning rates from radial burning motor test data are not accurate enough to provide a conclusive comparison with the burning rates of solid propellant strands. Furthermore, I think that a radial burning grain providing a progressive pressure-time trace should not be used in further testing of this comparative nature. This is due to the difficulties involved in obtaining reproducible, uniform ignition of the grain. A system providing a relatively soft and controllable energy impulse for ignition would be a worthwhile research tool for studies of this type. If this ignition system were available, a radial burning grain might still be useful if propellant reproducibility and/or recording instrumentation error problems could be solved.

III. Conclusions and Suggestions for Further Research

There has been some evidence in the outside literature that at chamber pressures less than 350 psi, the combustion efficiency of the solid propellant, and the resulting value of c*, is low. These experimental results tend to bear out the correctness of this evidence since low values of c*, at the lower chamber pressures, would lower the average c* for the rocket test and depress the calculated burning rates. This would tend to explain the low burning rates determined from these motor tests, but as yet no certain explanation is available to explain the low combustion efficiencies at low chamber pressures.

Further rocket motor tests using grains with a neutral burning characteristic should be made to test experimentally the validity of the conclusion that using a radial burning grain to determine propellant burning rates as a function of pressure is unreliable and irreproducible.

It is further suggested that the combustion mechanism of composite solid propellants at pressures below 400 psia be investigated. This should be done to explain the very large discrepancy in strand and motor burning rates and determine the reason for the low values of c* in the pressure range from atmospheric pressure to 400 psia.

In conclusion it may be said that present strand burning rate measurement techniques produce more reliable data than rocket motor tests using radial burning grains. The amount of radiant energy feedback to the burning solid propellant was found in strands to be about a third of that in a rocket motor having combustion taking place on surfaces inside the grain. The experimental measurement of the radiant energy feedback in a rocket motor grain showed that the analytical calculation was essentially correct. Unfortunately no conclusions may be drawn as to the validity of the

Summerfield granular diffusion flame theory for prediction of composite propellant burning rates in a radial burning rocket motor. It is also impossible to determine the reason for the increased propellant burning rates in a rocket or "scale" effect as observed by other research. Our tests were unable to provide an accurate comparison of solid propellant burning rates in rocket motors and strands. Consequently, the previously suggested new research should be carried out to explain our present test results.

REFERENCES

1. Summerfield, M., Sutherland, G. S., Webb, M. J. Taback, H. J., Hall, K. P., "Burning Mechanism of Ammonium Perchlorate Propellants," ARS Preprint 737-58.

2. Blair, D. W., Bastress, E. K., Hermance, C. E., Hall, K. P. Summerfield, M., " Some Research Problems in the Steady State Burning of Composite Solid Propellants," ARS Preprint 1060-60

3. Webb, M. J., "The Dependence of Linear Burning Rate upon Pressure for Ammonium Perchlorate-Polyester Pesin Composite Propellant." M.S.E. Thesis, Aeronautical Engineering, Princeton, 1958.

4. Taback, H. J., "The Effects of Several Composition Factors on the Burning Rate of an Ammonium Perchlorate Solid Propellant." M.S.E. Thesis, Aeronautical Engineering, Princeton, 1958.

5. Sutherland, G. S., "Mechanism of Combustion of an Ammonium Perchlorate-Polyester Resin Composite Solid Propellant." Ph D. Thesis, Aeronautical Engineering, Princeton, 1956.

6. Sutton, George, "Rocket Propulsion Elements," John Wiley and Sons, New York, 2nd Ed.,

7. Mahaffy, D. A., "Experimental Determination of Combustion Temperatures of Ammonium Perchlorate Propellants". M.S.E. Thesis, Aeronautical Engineering, Princeton, 1955.

8. Bartley, C. E., "Application of Simplified Method for Determining the Internal Ballistics Characteristics of Solid Propellants," Jet Propulsion Laboratory, California Institute of Technology, Progress Report No. 20-153, November 6, 1951.

9. Blair, D. W., Unpublished research for PhD. Thesis for Columbia University; to be published within a year.

10. Summerfield, Martin, "Burning Rate Theory for Composite Solid Propellants With Radiative and Conductive Energy Transfer to the Solid Surface," Unpublished Paper, Guggenheim Jet Propeusion Center, Princeton University.

11. Project Squid, Semi-Annual Progress Report, October 1, 1959, Princeton University Report.

12. Penner, S. S., "Emission of Radiation of Diatomic Gases," Journal of Applied Physics, 21, 1950, p.685

13. Penner, S. S., "Qualitative Molecular Spectroscopy and Gas Emmisivities," Addison-Wesley, Reading, Massachusetts.

14. McAdams, W. H., "Heat Transmissio " McGraw-Hill, New York, 3rd Ed., 82-86

15. Moelwyn Hughes, E. A., "Physical Chemistry," Pergamon Press; p. 400, 405

16. Eckert and Drake, "Heat and Mass Transfer," McGraw Hill, 2nd Ed., chp. 13-14

17. Beers, Yardley, "Introduction to the Theory of Error," Addison-Wesley, Reading, Massachusetts.

APPENDIX I:

TABLE I: Final Design Dimensions for Rocket Motor and Grains

A. Rocket Motor Dimensions

Overall Length	11.75 in.
Outside Diameter	4.125 in.
Inside Diameter	3.625 in.
Combustion Chamber Length	8.625 in.

B. Grain Dimensions

1. Low Pressure Grain:	d_p = 2.02 in. D = 3.40 in. L = 3.50 in.
2. Medium Pressure Grain	d_p = 1.33 in. D = 3.33 in. L = 2.84 in.
3. High Pressure Grain	d_p = 1.42 in. D = 2.40 in. L = 7.00 in.

C. Nozzle Diameters

1. Low Pressure	d_t = 0.640 in.
2. Medium Pressure	d_t = 0.422 in.
3. High Pressure	d_t = 0.452 in.

TABLE II. Density of Rocket Motor Propellant from Propellant Several Batches

Batch No.	Density #/in^3
50	0.0616
54	0.0616
55	0.0618
56	0.0620
56	0.0614
56	0.0616

Average Density: 0.0616 ± 0.0004 #/in^3

Note: Density variation is within the limits of measuring error due to weighing apparatus. Fluid used to determine propellant density was a naptha type fluid, "Skellysolve C." The average propellant density was determined by these tests and used in burning rate computations.

Derivation of Equation for Nozzle Throat Diameter from Design Conditions

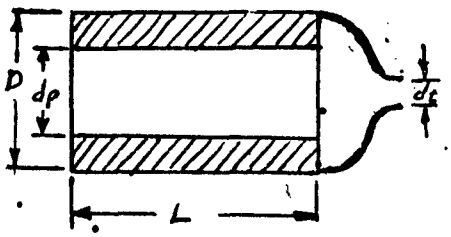

$$m = \rho_p L \frac{\pi}{4}(D^2 - d_p^2)$$

$$K_{N_1} = \frac{A_{Burning}}{A_t} = \frac{4 d_p L}{d_t^2}$$

$$K_{N_2} = \frac{4DL}{d_t^2}$$

$$d_p = \sqrt{10}\, d_t$$

$$m = \rho_p \frac{\pi}{4} \frac{d_p d_t^2}{4} K_{N_1}\left(\frac{K_{N_2}^2}{K_{N_1}^2} - 1\right)$$

$$m = \sqrt{10}\, d_t^3 \frac{\rho_p \pi K_{N_1}}{16}\left[\left(\frac{K_{N_2}}{K_{N_1}}\right)^2 - 1\right]$$

$$d_t = \left(\frac{16\, m}{\sqrt{10}\, \rho_p \pi K_{N_1}\left[\left(\frac{K_{N_2}}{K_{N_1}}\right)^2 - 1\right]}\right)^{1/3}$$

APPENDIX II: I. Data Reduction Procedure: Calculation of Burning Rates from Rocket Motor Tests

As previously explained, the burning rate of the solid propellant in a radial burning grain may be calculated by determining an expression for the radius of the burning surface and differentiating this expression with respect to time. The derivation of this procedure is as follows and is similar to the method in (8).

Equate the rate of combustion gas generation from the solid propellant to the gas flow rate out the nozzle plus the rate of increase of the combustion gas mass inside the combustion chamber.

$$\dot{m} = A_b \rho_p r_i = \frac{d}{dt}(\rho_c V_c) + \frac{A_t g P_c}{c^*} \tag{1}$$

For a first approximation, assume $\frac{d}{dt}(\rho_c V_c) = 0$, then

$$A_b \rho_p r_i = \frac{A_t g P_c}{c^*} \tag{2}$$

and substituting $r_i = dR/dt$ and $A_b = 2\pi RL$, we get

$$2\pi RL \rho_p \, dR/dt = \frac{A_t g P_c}{c^*} \tag{3}$$

$$\int_{R_o}^{R_i} R\,dR = \int_0^{t_i} \frac{A_t g}{2\pi L \rho_p} \frac{P_c}{c^*} dt \tag{4}$$

Integrating, taking the square root and letting $\eta = \frac{A_t g}{2\pi L \rho_p}$ we obtain

$$R_i = \left(\frac{2\eta}{c^*} \int_0^{t_i} P_c dt + R_o^2 \right)^{1/2} \tag{5}$$

and

$$\frac{dR_i}{dt} = r_i = \frac{\eta P_{c_i}}{c^* \left(\frac{2\eta}{c^*} \int_0^{t_i} P_c dt + R_o^2 \right)^{1/2}} \tag{6}$$

The value of η is known and constant for each particular nozzle diameter and grain configuration, c* is the average, experimental c* determined from the equation

$$c^* = \frac{A_t g \int_0^{t_{final}} P_c dt}{W} \tag{7}$$

and R_o is initial grain port diameter and a constant for each grain.

Hence by calculating the area under the experimental pressure time curve on rectilinear paper up to a time t_i, the burning rate, r_i, may be found for the instantaneous chamber pressure, P_{c_i} at time t_i.

It should be noted that there exists another method of calculating the instantaneous burning rate using the relations:

$$P_c = f(K_N) \tag{8}$$

$$K_N = \frac{A_p}{A_t} \tag{9}$$

$$r = \frac{A_t}{2\pi L f'(K_N)} \frac{dP_{c_i}}{dt} \tag{10}$$

This method requires taking two derivatives from experimental curves which is not a process that may be done accurately. The advantage to the integral method used in the data reduction is that integration of data is a stabilizing process and may be much more accurately done than the determination of the slope of an experimental line.

APPENDIX II: 2. Δr Due to Rate of Gas Mass Increase in Combustion Chamber

The effect of neglecting the term $\frac{d}{dt}(\rho_c V_c)$ in Equation (1) may be investigated in the following manner. The effect of excluding the term $\frac{d}{dt}(\rho_c V_c)$ is to decrease the rate at which the propellant produces gas or to decrease the apparent, calculated burning rate. Hence to determine the effect of the term $\frac{d}{dt}(\rho_c V_c)$ we may write an expression $(r - r_o) A_b \rho_p$ which is the increase in the rate of propellant gas production. Here r_o is the apparent burning rate neglecting $\frac{d}{dt}(\rho_c V_c)$ and r is the actual burning rate. We may then say that

$$(r - r_o) A_b \rho_p = \frac{d}{dt}(\rho_c V_c) \tag{11}$$

$$\frac{d}{dt}(\rho_c V_c) = V_c \frac{d\rho_c}{dt} + \rho_c \frac{dV_c}{dt} \tag{12}$$

Combining Equations (11) and (12) we obtain

$$(r - r_o) A_b \rho_p = V_c \frac{d\rho_c}{dt} + \rho_c \frac{dV_c}{dt} \tag{13}$$

The term $\rho_c \, dV_c/dt$ is the increase in gas mass due to volume change of the combustion chamber. Since this term is small we will approximate it by saying it is equal to the volume change of the grain associated with the apparent burning rate r_o. Then

$$\rho_c \frac{dV_c}{dt} \doteq \rho_c A_b r_o \tag{14}$$

With this approximation for V_c, the term $V_c \, d\rho_c/dt$ becomes

$$V_c \frac{d\rho_c}{dt} \doteq \left(V_{c_{initial}} + \int_0^{t_i} A_b r_o \, dt\right) \frac{d\rho_c}{dt} \tag{15}$$

Substituting Equations (14) and (15) into Equation (13) and dividing by $A_b \rho_p$ results in

$$(r - r_o) = \Delta r = \frac{\left(V_{c,initial} + \int_0^{t_i} A_b r_o \, dt\right)}{A_b \rho_p R T} \frac{dP_c}{dt} + \frac{r_o P_c}{\rho_p} \quad . \tag{16}$$

Calculation of Δr for a typical motor test showed that it was of a constant value of +1% over the entire pressure range. Thus the effect of neglecting the term $\frac{d}{dt}(P_c V_c)$ of Equation (1) is indeed negligible and will little affect the comparison of burning rates in rocket motors and strands.

APPENDIX II: 3. Error Analysis of Data Reduction Procedure

The burning rate of composite propellant in the rocket motor is a function $r = r(L, P_c, C^*, R_o, A_t, \int_o^t P_c dt, \rho)$. Specifically, r may be explicitely written as

$$r = \frac{A_t g P_c}{2\pi L \rho C^{*1/2} \left(\frac{A_t g}{\pi L \rho}\int_o^t P_c dt + C^* R_o^2\right)^{1/2}} ; \quad a = \int_o^t P_c dt$$

while c* may be written as

$$C^* = \frac{A_t g \int_o^{t_{final}} P_c dt}{W}$$

Since the errors involved in calculating (r) are independent, we may write that the standard deviation of the burning rate, S_r, is, Reference (17),

$$S_r = \sqrt{\left(\frac{\partial r}{\partial L}\right)^2 S_L^2 + \left(\frac{\partial r}{\partial P_c}\right)^2 S_{P_c}^2 + \left(\frac{\partial r}{\partial C^*}\right)^2 S_{C^*}^2 + \left(\frac{\partial r}{\partial R_o}\right)^2 S_{R_o}^2 + \left(\frac{\partial r}{\partial A_t}\right)^2 S_{A_t}^2 + \left(\frac{\partial r}{\partial a}\right)^2 S_a^2 + \left(\frac{\partial r}{\partial \rho}\right)^2 S_\rho^2}$$

$S_L \hat{=} (\delta L)$ $\quad \delta L = \pm 0.01$

$S_{P_c} = \sqrt{\frac{\sum_i^4 (\delta P_c)^2}{4}}$ $\quad \delta P_c = \pm 10$

$S_{C^*} = \sqrt{\left(\frac{\partial C^*}{\partial A_t}\right)^2 S_{A_t}^2 + \left(\frac{\partial C^*}{\partial d_t}\right)^2 S_{d_t}^2 + \left(\frac{\partial C^*}{\partial W}\right)^2 S_W^2}$

$S_{R_o} \hat{=} .5 R_o$ $\quad \delta R_o = \pm 0.05$

$S_{A_t} = \sqrt{\left(\frac{\pi d_t}{2}\right)^2 \delta_{d_t}^2}$ $\quad \delta_{dt} = \begin{cases} 1.4 \times 10^{-3} & \text{Contraction due to heating} \\ 10^{-3} & \text{No contraction due to heating} \end{cases}$

$S_a \hat{=} \delta a \doteq \sum_i (P_{c_i} \delta_{\Delta t_i} + \delta P_i \Delta t_i)$

$S_\rho \hat{=} \delta \rho$ $\quad \delta \rho = \pm 0.003$

$S_W \hat{=} \delta W$ $\quad \delta W = \pm 0.1$

S_{A_t} has two values depending on whether or not contraction of the nozzle during firing is considered. For an order of magnitude approximation of the amount the nozzle diameter might change during a run, it is assumed that the nozzle reaches the temperature of 2000°R to a depth of 0.1 inches during the motor test. If the temperature coefficient of expansion of the Mb and the Cu is assumed to be approximately 7×10^{-6} in/in°F, the $S^2_{A_t}$ due to nozzle contraction is 1.96×10^{-6} compared to $S^2_{A_t}$ of 0.159×10^{-6} for the zero contraction case.

Calculation of the necessary partial derivatives of the burning rate $\left(\frac{\partial r}{\partial \chi_i}\right)$ and the associated values of standard deviation S_{χ_i} are tabulated in the following table.

Error Quantity Tabulation

Variable, χ_i	$\left(\frac{\partial r}{\partial \chi_i}\right)$	$\left(\frac{\partial r}{\partial \chi_i}\right)^2$	$S^2_{\chi_i}$	$\left(\frac{\partial r}{\partial \chi_i}\right)^2 S^2_{\chi_i}$	
L	0.132	0.0174	10^{-4}	1.74×10^{-6}	
P_c	3.06×10^{-4}	9.38×10^{-8}	1.25×10^{2}	11.72×10^{-6}	
c*	0.431×10^{-5}	0.186×10^{-10}	7.52×10^{6}	1.4×10^{-4}	Nozzle Contraction
			7.35×10^{6}	1.37×10^{-4}	No Nozzle Contraction
R_o	0.218	0.0475	2.5×10^{3}	0.0118×10^{-6}	
A_t	4.78	22.2	0.312×10^{-6}	6.84×10^{-6}	Nozzle Contraction
			$0.159\times$	3.53×10^{-6}	No Nozzle Contraction
a	1.04×10^{-4}	1.08×10^{-8}	2.29×10^{3}	24.7×10^{-6}	
ρ	5.2	27	9×10^{6}	2.43×10^{-4}	

The standard deviation of the burning rate, $S_r = \sqrt{\sum_{\chi_i} \left(\frac{\partial r}{\partial \chi_i}\right)^2 S_{\chi_i}^2}$

S_r is the standard deviation. The percent error associated with the burning rate determination is shown in the table below:

Case	S_r	% Error in (r); $\frac{S_r}{r} \times 100$
1) No Nozzle Contraction (due to heating)	2.052×10^{-2}	6.70%
2) Nozzle Contraction (due to heating)	2.07×10^{-2}	6.76%

The percent error in the calculated motor burning rate due to the possible error in the variables χ_i may be determined in the following manner. Consider that the burning rate standard deviation S_r is a vector whose coordinates are the errors in the quantities χ_i. For example, assume P, P_c, and c* are the variables χ_i.

$$\bar{S}_r = A\bar{e}_\rho + B\bar{e}_{P_c} + C\bar{e}_{c^*}$$

$$|S_r| = \sqrt{|A|^2 + |B|^2 + |C|^2} = \sqrt{\left(\frac{\partial r}{\partial \rho}\right)^2 S_\rho^2 + \left(\frac{\partial r}{\partial P_c}\right)^2 S_{P_c}^2 + \left(\frac{\partial r}{\partial c^*}\right)^2 S_{c^*}^2}$$

The associated direction cosines are thus

$$\cos(\alpha_\rho) = \frac{|A|}{|\bar{S}_r|}, \text{ etc.}$$

The fraction of $\bar{S}_r$ due to A, F_ρ, is then $|A|\cos\alpha_\rho = \frac{|A|^2}{|\bar{S}_r|}$

Then the amount of $\bar{S}_r$ due to A is thus $F_\rho \cdot |\bar{S}_r| = \Delta_\rho = |A|^2/|\bar{S}_r|$

and similarly for the other variables. The percent change in motor burning rate is therefore $\frac{\Delta \chi_i}{r} \times 100$ % for each variable χ_i. These percentages are tabulated below:

% Error in (r_{avg}) due to Error in Variable

Variable, χ_i	$\Delta\chi_i$	$\%\Delta r = \frac{\Delta\chi_i}{r_{avg}} \times 100$, $r_{avg} = 0.306$	
		No Nozzle Contraction	Nozzle Contraction
L	0.84×10^{-4}	.0272	0.0271
P_c	5.67×10^{-4}	.1855	0.185
C*	67.6×10^{-4} 66.8×10^{-4}	2.190	2.220
R_o	0.00561×10^{-4}	0.0001	0.0001
A_t	3.3×10^{-4} 1.72×10^{-4}	0.0564	0.111
a	11.95×10^{-4}	0.392	0.392
ρ	117.5×10^{-4}	3.850	3.950
		6.7000	6.7620

It is therefore evident that the largest single errors in motor burning rate determination are errors in propellant density and in c* determination.

APPENDIX II: 4. Motor Burning Rate Uncertainty Analysis

$A_b r \rho = K P_c$; K = constant

Let $A = 2\pi L \bar{R}$ be the cylindrical area associated with a cylinder of mean radius $\bar{R}$, and differentiate above equation with respect to time, noting that $r = \frac{d\bar{R}}{dt}$. Assume that r may be described by $r = a p^n$. Then

$$\frac{dr}{dt} = a n p^{n-1} \frac{dp}{dt} = \left(\frac{nr}{p}\right)\frac{dp}{dt}$$

$$r^2 + \frac{\bar{R} n r}{p}\frac{dp}{dt} = \frac{k}{2\pi L \rho}\frac{dp}{dt}$$

$$r^2 = \left(\frac{k}{2\pi L \rho} - \frac{\bar{R} n r}{p}\right)\frac{dp}{dt}$$

$$r^2 = \left(\frac{2\pi L \rho \bar{R} r}{2\pi L \rho p} - n\frac{\bar{R} r}{p}\right)\frac{dp}{dt}$$

$$r^2 = \frac{r\bar{R}}{p}(1-n)\frac{dp}{dt}$$

$$r = \frac{(1-n)\bar{R}}{p}\frac{dp}{dt}$$

At a constant chamber pressure, picked for comparison of pressure time curves, $dp = 0$. Therefore the variation of r at this pressure, Δr is:

$$\Delta r = \left(\frac{\partial r}{\partial p}\right)^{0} dp + \frac{\partial r}{\partial\left(\frac{dp}{dt}\right)} \Delta\left(\frac{dp}{dt}\right)$$

$$\Delta r = \frac{(1-n)\bar{R}}{p}\Delta\left(\frac{dp}{dt}\right)$$

$$\frac{\Delta r}{r} = \frac{\Delta\left(\frac{dp}{dt}\right)}{\left(\frac{dp}{dt}\right)}$$

The last equation shows that the test to test percent variation in $\frac{\Delta r}{r}$ at a particular chamber pressure is equal to the percent variation in the slope, $\left(\frac{dP}{dt}\right)$, at that pressure.

The data on $\left(\frac{dP}{dt}\right)$ resulting from the rocket motor tests reported herein is presented below:

Medium Pressure Grain and 0.25" Diameter Nozzle		Low Pressure Grain and 0.359" Diameter Nozzle	
$P_{chamber}$, psig	dP/dt	$P_{chamber}$, psig	dP/dt
900	2.32	900	1.07
900	2.72	900	1.24
900	2.85	900	2.5
900	2.2		
600	1.75	600	0.90
600	2.22	600	0.98
600	2.1	600	0.93
600	1.52		

APPENDIX III: I. Calculation of Radiant Energy Flux to Grain Burning Surface

To approximate the amount of heat transfecred back to the flame of the burning hollow charge of a solid propellant due to the core of hot exhaust gases we may use the equation

$$\dot{q} = \bar{\epsilon} \sigma T_g^4$$

According to Reference (7), the quantities of significantly radiating exhaust gases are:

0.383 moles CO_2

2.067 moles CO

1.583 moles H_2O

0.975 moles HCl

in a total number of moles of products of 6.483.

Assume that the height of the grain in question is 5 inches with an inside diameter of 2 3/4 inches. The equivalent radius L_e is given by Reference (16) as $0.9\left(\frac{4V}{A_{surface}}\right)$

For the concave grain surface area,

$$L_e = (0.9)(4)\frac{(h\,\pi d^2/4)}{\pi d h} = 0.9d = 0.2 \text{ ft.}$$

$$\frac{PP_{CO_2}}{P_T} = \frac{0.383}{6.483} = 0.0591$$

$$\frac{PP_{H_2O}}{P_T} = \frac{1.583}{6.483} = 0.244$$

$$\frac{PP_{CO}}{P_T} = \frac{2.067}{6.483} = 0.319$$

$$\frac{PP_{HCl}}{P_T} = \frac{0.975}{6.483} = 0.151$$

Emissivity for Pure Gases - Estimation (Reference 12)

$$\epsilon' = [1-\exp(-k_F P\ell)] \frac{\sum_n \int_{\Delta\nu_{n\to n+1}} p(\nu)d\nu}{\int_0^\infty p(\nu)\,d\nu}$$

$$+ [1-\exp(-k_{FO} P\ell)] \frac{\sum_n \int_{\Delta\nu_{n\to n+1}} p(\nu)d\nu}{\int_0^\infty p(\nu)\,d\nu} + \cdots\cdots$$

$$\epsilon' = [1-\exp(-k_F P\ell)]\,\epsilon'_F + [1-\exp(-k_{FO} P\ell)]\,\epsilon_{FO} + \cdots\cdots$$

where k_i is average absorption coefficient for i^{th} vibration rotation band, P = partial pressure of absorber, and ℓ = optical path length.

$$k_F = \frac{1}{\Delta\nu_{n\to n+1}} \sum_n \sum_j \left(\int_{\substack{n\to n+1 \\ j\to j-1}} P_\nu d\nu + \int_{\substack{n\to n+2 \\ j-1\to j}} P_\nu d\nu \right) = \frac{\alpha_{o1}}{\Delta\nu_{n\to n+1}}$$

$$k_{FO} = \frac{\alpha_{o2}}{\Delta\nu_{n\to n+2}}$$

where α_{oi} is the integrated absorption coefficient.

There is a restriction that $P_\nu P\ell \ll 1$ but the same equations may also be used when the total pressure is high as proved using Elasser's theoretical treatment for equally intense, equally spaced rotational lines. We may also write that

$$k_F = \frac{N_T \pi \epsilon_F^2}{3\mu c \Delta\nu_{n\to n+1}} = \frac{\alpha_{o1}}{\Delta\nu_{n\to n+1}} \; ; \; N_T = \frac{7.34\times10^{21}}{T} \frac{\text{molecules}}{\text{cc atm.}}$$

Hence:

$$\frac{k_F(T_1)}{k_F(T_2)} = \frac{T_2}{T_1} \frac{\Delta\nu_{n\to n+1}(T_2)}{\Delta\nu_{n\to n+1}(T_1)} \; , \; \frac{k_{FO}(T_1)}{k_{FO}(T_2)} = \frac{T_2}{T_1} \frac{\Delta\nu_{n\to n+2}(T_2)}{\Delta\nu_{n\to n+2}(T_1)}$$

$$\frac{K_{FO}}{K_F} = \frac{\chi_e(1-5\chi_e)}{(1-3\chi_e)^2} \; ; \; \chi_e = \text{anharmonicity constant of molecule under consideration}$$

Calculation of ϵ_T for CO

$$\frac{k_F(T_1)}{k_F(T_2)} = \frac{T_2}{T_1}\frac{\Delta\nu_{n\to n+1}(T_2)}{\Delta\nu_{n\to n+1}(T_1)} \qquad k_F(T_1) = \frac{\alpha_{01}(T_1)}{\Delta\nu_{n\to n+1}(T_1)}$$

$$K_F(300) = \frac{1.182\times10^{13}(\text{cm atm})^{-1}\text{sec}^{-1}}{214\,\text{cm}^{-1}\cdot 3\times10^{10}\,\text{cm sec}^{-1}}$$

$$K_F(300) = 18.43\ (\text{cm atm})^{-1}$$

$$K_F(T_2) = \frac{k_F(T_1)[T_1\Delta\nu_{n\to n+1}(T_1)]}{T_2[\Delta\nu_{n\to n+2}(T_2)]}$$

$$\underline{K_F(3000) = 0.626\ (\text{cm atm})^{-1}}$$

$$K_{FO}(300) = \frac{\alpha_{02}(T_1)}{\Delta\nu_{n\to n+2}} = \frac{1.54\times10^{11}}{213\times3\times10^{10}}$$

$$K_{FO}(300) = 0.0241\ (\text{cm atm})^{-1}$$

$$K_{FO}(T_2) = \frac{k_{FO}(T_1)[T_1\Delta\nu_{n\to n+2}(T_1)]}{T_2[\Delta\nu_{n\to n+2}]}$$

$$K_{FO}(3000) = 1.85\times10^{-4}\ (\text{cm atm})^{-1}$$

Compare ϵ_{CO} at two pressures, 500 psi = 34 atm and 1000 psig ≈ 68 atm.

$$\frac{PP_{CO}}{P_T} = 0.319$$

$$PP_{CO}^{500} = 34(0.319) = 10.85 \text{ atm}$$

$$PP_{CO}^{1000} = 68(0.319) = 21.7 \text{ atm}$$

Optical Path: ℓ_1 = 0.2 ft. to cylindrical surface

$$PP_{CO}^{1}\ell_1 = 2.17 \text{ ft atm} = (2.17)(12 \times 2.54) = 66.2 \text{ cm atm}$$

$$PP_{CO}^{2}\ell_1 = 4.34 \text{ ft atm} = 132.4 \text{ cm atm}$$

Reference (12) gives data for CO partial emissivities at values of 5 ft atm.

Hence calculate at this point:

$$T = 2800°K \quad \epsilon'_{F_{CO}} \cong 0.03 \quad \epsilon'_{FO_{CO}} \cong 0.07$$

$$\left(\epsilon'_{T_{CO}}\right)_{\substack{1000 \text{ psi} \\ 2800°K}} = \left[1 - \exp(-0.626 \times 132.4)\right]0.03 + \left[1 - \exp(-0.185 \times 132.4)\right]0.07$$

$$\approx 0.03 + 0.00167$$

$$\epsilon'_{T_{CO}} = 0.0317 \text{ ; 1000 psi and } 2800°K$$

We may note however, that the band width does not rapidly change with elevated total pressure and relatively high values of absorber partial pressure. Hence the emissivity of CO at 500 psig may be estimated using the same data for $\epsilon'_{F_{CO}}$ and $\epsilon'_{FO_{CO}}$ as at 1000 Psig.

$$\left(\epsilon'_{T_{CO}}\right)_{\substack{500\,psi \\ 2800\,^\circ K}} = \left[1-\exp(-0.626\times 66.2)\right]0.03 + \left[1-\exp(-0.185\times 10^{-3}\times 66.2\right]0.07$$

$$= 0.02955 + 0.00089$$

$$\epsilon'_{T_{CO}} = 0.0304 \quad ,\ 500\,psi \text{ and } 2800^\circ K$$

Calculation of ϵ_{HCl}:

Reference (12) shows that K_{FO} for HCl may be directly calculated from spectral data providing K_F is known by the equation

$$\frac{K_{FO}}{K_F} = \frac{\chi_e(1-5\chi_e)}{(1-3\chi_e)^2}$$

where χ_e is the anharmonicity constant of the HCl molecule. The value of χ_e may be computed as being 1.793×10^{-2}, (15).

$$\frac{K_{FO}}{K_F} = 1.82\times 10^{-2}$$

$$K_F = \frac{7.34\pi\times 10^{21}\epsilon_F^2}{3\mu C T} = 11.38\times 10^{-3}\ (cm\ atm)^{-1}$$

$$K_{FO} = 20.7\times 10^{-5}\ (cm\ atm)^{-1}$$

$PP^1_{HCl} = 0.151(34) = 5.14$ atm

$PP^2_{HCl} = 10.28$ atm

$PP^1_{HCl} \cdot l_1 = 1.023$ ft atm $= 31.3$ cm atm

$PP^2_{HCl} l_1 = 62.6$ cm atm.

Total Pressure of 500 psi:

$$\epsilon_{T_{HCl}} = [1 - \exp(-1.138\times10^{-2}\times31.3)]0.07 + [1 - \exp(-2.07\times10^{-4}\times31.3)]0.172$$

$$\epsilon_{T_{HCl}} = 0.0318$$

Total Pressure of 1000 psi:

$$\epsilon_{T_{HCl}} = [1 - \exp(-1.138\times10^{-2}\times62.6)]0.07 + [1 - \exp(-2.07\times10^{-4}\times62.6)]0.172$$

$$\epsilon_{T_{HCl}} = 0.0379$$

Heat transfer calculation, $P_T = 1000$ psi, $T = 2800°K$:

$PP_{CO_2} = 1.02$ atm. $PP_{H_2O} = 16.6$ atm $PP_{H_2O} + P_T = 84.6$ atm

$PP_{CO_2} l_e = 0.802$ ft atm $PP_{H_2O} l_e = 3.32$ ft atm $PP_{H_2O} l_e \cong 3$ ft atm

$\epsilon'_{CO_2} = 0.098$ $\epsilon'_{H_2O} = 0.14$ $C_W \cong 1.3$

$\epsilon_{H_2O} \cong 0.182$

$\frac{PP_{H_2O}}{PP_{H_2O} + PP_{CO_2}} = 0.806$ $\therefore \Delta\epsilon$ correction for H_2O and CO_2 together $\cong -0.09$

$\epsilon_T (H_2O \text{ and } CO_2) = 0.1472$

$\epsilon_T = \epsilon_{T_{H_2O+CO_2}} + \epsilon_{HCl} + \epsilon_{CO} = 0.2168$

$\dot{q} = \epsilon_T \sigma T_g^4 = 76.4$ watts/cm^2 to cylindrical surface

Now compute q for 500 psia, and 2800°K:

$$PP_{CO_2} = 2.01 \text{ atm} \qquad P.P_{CO_2} l_e = 0.402 \text{ ft atm}$$

From extension of Hottel charts, ϵ'_{CO_2} @ 0.4 ft atm and 5000°R = 0.034. $C_c \cong 1.2$

$$\therefore \epsilon_{CO_2} \cong 0.0408$$

$$PP_{H_2O} = 8.29 \text{ atm} \qquad PP_{H_2O} l_e = 1.66 \text{ ft atm}$$

$$\epsilon_{H_2O} = 0.094 \text{ , } 5000°R \text{ and } 1.66 \text{ ft atm}$$

Correction is determined from (14).

$$PP_{H_2O} + P_T = 36.01 \text{ atms}$$

$$PP_{H_2O} l_e \cong 1.5$$

Hence extrapolation for correction factor C_W from Reference (14) gives $C_W \cong 1.4$

$$\therefore \epsilon_{T_{H_2O}} \cong 0.132$$

The corrections for having both CO_2 and H_2O present, calculated from Reference (14) is determined for $\dfrac{PP_{H_2O}}{PP_{CO_2} + PP_{H_2O}} = 0.805$

$$\therefore \Delta\epsilon_{correction} \cong -0.09$$

$$\epsilon_{T(H_2O + CO_2)} = 0.0828$$

$$\epsilon_T = \epsilon_{\substack{CO_2 \\ +H_2O}} + C_{HCl} + \epsilon_{CO} = 0.145$$

$$q = \epsilon_T \sigma T_g^4$$

$q = 51.0$ watts/cm² to cylindrical surface.

APPENDIX III: 2. Prodiction of Radiant Energy Received by Radiation Thermocouple Dusing Motor Test and Comparison with Experimental Results

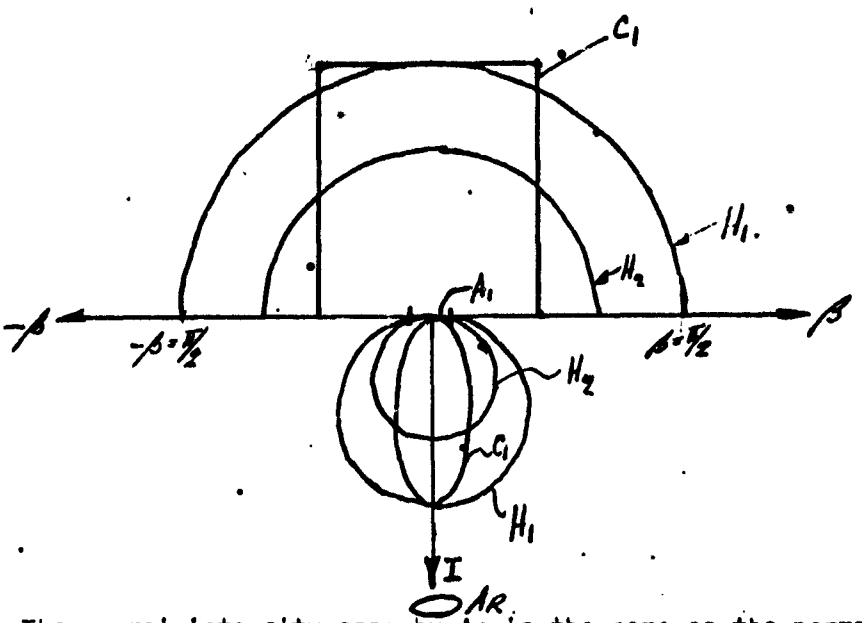

The normal intensity seen by A_R is the same as the normal intensity from the hemisphere of radiating gas H_1. Total heat transferred to A_1 by cylinder C_1 is the same as heat transferred by equivalent hemisphere of radiating gas H_2. For purposes of computing the heat transferred to elemental area A_R from elemental area A_1, we are only concerned with the normal radiation intensity through area A_1 due to the cylinder of gas C_1. This normal radiation intensity is identical to the normal intensity due to the hemisphere H_1.

The total heat radiated from the cylinder C_1 equals the total heat radiated from the equivalent hemisphere H_2 but the normal intensity from C_1 is the same as the normal intensity from H_1. Since the heat transferred to the area A_R is a function only of the normal intensity from C_1, we need only compute the normal intensity of the hemisphere H_1 to compute the heat transferred to A_R. This normal intensity is defined as the heat transferred to A_1 divided

by π . The calculation is as follows for a total pressure of 500 psi and a flame temperature of 2800°K. The radius of H_1 is assumed to be 7.2 inches.

ϵ_{CO_2} calculation:

$PP_{CO_2} = 4.02$ atm

$PP_{CO_2} L = 2.42$ ft atm

$\epsilon'_{CO_2} = 0.068$

$C_{CO_2} \cong 1.11$

$\epsilon_{CO_2} = 0.0735$

ϵ_{H_2O} calculation:

$PP_{H_2O} = 16.6$ atm

$PP_{H_2O} L = 10.0$ ft atm

$\epsilon''_{H_2O} = 0.190$

$C_{H_2O,\ \text{pressure correction}} \cong 1.4$

$\epsilon'_{H_2O} = 0.266$

$PP_{H_2O} + P_T = 50.6$ atm

$\dfrac{PP_{H_2O}}{PP_{H_2O} + PP_{CO_2}} = 0.805$

$\Delta\epsilon_{CO_2+H_2O} \cong -0.10$

ϵ calculation for combined CO_2 and H_2O :

$$\epsilon_{CO_2+H_2O} = 0.0735 + 0.266 - 0.10 = 0.2395$$

ϵ_{CO} calculation:

$K_F = 0.626$ (cm atm)$^{-1}$

$K_{FO} = 1.85 \times 10^{-4}$ (cm atm)

$PP_{CO} L = 6.54$ ft atm $= 199.0$ cm atm

$$\epsilon_{CO} = [1 - \exp(-0.626 \times 199)]\,0.03 + [1 - \exp(-1.85 \times 10^{-4} \times 199)]\,0.07$$

$$\epsilon_{CO} = 0.0326$$

ϵ_{HCl} calculation: $K_F = 11.38 \times 10^{-3}$ (cm atm)$^{-1}$ $\quad PP_{HCl} \cdot L = 3.07$ ft atm

$K_F = 2.07 \times 10^{-1}$ (cm atm)$^{-1}$ $\quad PP_{HCl} \cdot L = 93.5$ cm atm

$$\epsilon_{HCl} = [1 - \exp(-1.138 \times 10^{-2} \times 93.5)]0.07 + [1 - \exp(-2.07 \times 10^{-1} \times 93.5)]0.172$$

$$\epsilon_{HCl} = 0.049$$

Total Emissivity, Heat Transfer, and Normal Intensity:

$$\epsilon_T = \epsilon_{CO_2 + H_2O} + \epsilon_{CO} + \epsilon_{HCl}$$

$$\epsilon_T = 0.321$$

$$q = \epsilon \sigma T_g^4$$

$$q = 113 \text{ watts/cm}^2$$

$$I_N = \frac{q}{\pi} = 36.0 \frac{\text{watts/cm}^2}{\text{steradian}}$$

We are now in a position to predict the heat transfer that a receiver would experience when placed in the same position as the receiver in the experimental apparatus shown in Figure 26. The area which the radiation thermocouple sees is approximately described by the extreme rays of the aperture system. This diameter is 0.0904 inches or 0.23 cm, and the associated area is 0.0414 cm^2.

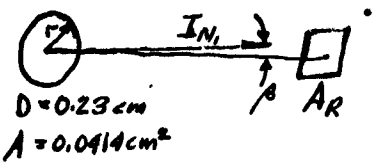

$$\left(\frac{dq_{1\to R}}{d\omega_R}\right) = I_N \cos\beta\, dA_1$$

$$\left(\frac{q_{1\to R}}{\omega_R}\right) = I_N A_1$$

$$\left(\frac{q_{1\to R}}{\omega_R}\right)_{Predicted} = 1.49 \text{ watts/steradian}$$

The radiant heat transfer to the radiation thermocouple measured by experiment is $\left(\frac{R_R}{A_R}\right)$. This may be converted to giving the radiation per steradian received from the emitting surface A_1 through the solid angle as follows:

$$\left(\frac{R_R}{\omega_1}\right) = \frac{R_R}{A_R/R^2} = \left(\frac{R_R}{A_R}\right)R^2$$

The average $\left(R_R/A_R\right)$ at approximately 500 psi experimentally found using KBr optics is 275 $\mu w/cm^2$.

$$\therefore \left(\frac{R_R}{\omega_1}\right)_{avg.} = (275\times10^{-6}\times3.820\times10^{3}) = 1.05 \text{ watts/steradian}$$

which is of the same order of magnitude as predicted. It is reasonable to assume that the method used to compute emissivities and heat transfer by radiation to the grain surface is approximately correct.

APPENDIX IV: Burning Rates Determined from Strands of Composite, Solid Propellant

1. Technique Development

In the research done on strand burning rates previous to the period starting in the fall of 1958, there was a relatively large amount of scatter in the data and the rate at which propellant strands could be made was low. Beginning in the fall of 1958, it was decided to undertake an examination of the radiation from the flame of a solid propellant strand. It became desirable to insure the uniformity of the propellant strands, increase the quantity of strands that could be made at one time, and improve the design and operation of the strand burner. These developments would increase the rate at which data could be obtained and reduce the scatter. The necessary techniques were mainly developed by D. W. Blair, (2), with some help from the author.

2. Strand Burner Design and Operation

The original strand burner design was modified by the introduction of a stainless steel tube or chimney surrounding the propellant strand, see Figures 1 and 2. The purge gas (nitrogen) flows into the chimney, up past the entire length of the strand and is exhausted at the top of the chimney. Flow rate of the purge gas, of the order of 3 ft/sec was controlled by means of a metering valve having a micrometer control allowing precise adjustment of the orifice opening. The purge gas flow was laminar at least up to the level of the burning surface of the strand. The chimney was, originally, to purge effectively the strand combustion products without disturbing the flame structure in order that the radiant energy emitted by the propellant flame might be observed. The use of the chimney greatly reduced the scatter

of burning rate data and was incorporated in all strand burning rate equipment.

Ignition was accomplished by means of a wire, passing through the top of the strand, which is heated electrically until enough heat is transferred to the strand to cause ignition. The burning surface of the strand progresses counter to the purge gas flow in the chimney. A water system was installed, Figure 1, and quench tests showed that when the ignition wire was carefully placed very near the strand's top and along a diameter of the strand, the burning surfaces obtained with the upward purge were quite flat and perpendicular to the strand axes, Figure 3. The burning rate of the strand was obtained by placing fusible wires at known distances along the strand and connecting the wires to a clock circuit. The melting of the wires stopped the associated clocks and hence the recording of elapsed time.

The possible errors in the system for obtaining strand burning rates were closely investigated at a standard pressure of 500 psig. Variation in purge velocity in the chimney ranging from 0.6 to 2.0 ft/sec did not affect the burning rate detectably. Purge gas for all pure burning rate tests was N2 but for radiation studies, up to 10% O_2 was added to get rid of the smoke in gas. The effect of O_2 concentration was investigated and found to be well within the statistical scatter, up to pure air concentrations. The standard burning rate determination method was to use strands inhibited on their surface with two coats of Testor's Butyrate Dope (Blue)--a model airplane lacquer, plus two coats of 5% Bakelite V.Y.L.F. plastic in methylene chloride. Checks of inhibited and uninhibited strands at 100 psig showed no significant difference in burning rate or in standard deviation of five runs for each strand type. The effect of strand diameter in 7/16 inch and 1/4 inch strands was tested

at 500 psig. The 7/16 inch diameter strands showed a 3% increase in burning rate over the 1/4 inch strands. This might be expected from the decreased convective heat loss as the strand diameter is increased.

3. Strand Manufacture

Strands were manufactured by mixing the propellant under vacuum and extruding the uncured propellant. The uncured propellant was placed in the extruder reservoir under vacuum, and extruded into wax molds from which strands were removed after curing was completed, Figure 4. When coarse oxidizer particle size was used, a settling of the oxidizer particles was noted when the strands were cured with the molds constantly in one position. This was avoided by constantly rotating the strands about their horizontal axis during the curing time. The possible effect of a separation of the fuel and oxidizer at molded surfaces was checked by casting the propellant into a 1x5x7 inch block and cutting out 1/4 inch strands after curing. At 500 psig the cut strands having at least one molded surface had burning rates identical with those of a standard cast strand but the strands cut from the inside of the block had a 7% lower burning rate. It was suggested that there was a separation of the fuel and oxidizer at a molded surface with the resultant higher oxidizer concentration within the strand, resulting in the higher burning rates of the extruded strands, but there is no direct proof for this.

4. Sources of Random Error

The preceding section dealt with the systematic errors involved in measuring the burning rate of solid propellant using the modified strand burner. The sources of random error were uncertainties in pressure on the burning surface of the strand, in timing wire placement, in timing clock

relay response, in the limits of clock reading accuracy, in the initial strand temperature, and in the uniformity of propellant. Webb (3) gives the random scatter due to these effects as 3.7%; 3.0% of this scatter Webb attributed to propellant non-uniformity. However, present propellant formulation and strand manufacturing techniques were more closely controlled than those of Webb and the random scatter due to propellant non-uniformity was reduced to ±1.0% or less. Taback (4) found that his known sources of error other than propellant non-uniformity accounted for 1.5 to 4% scatter over a pressure range of 30-1500 psig, while his experimental scatter was approximately twice that amount. Using the chimney purge strand burner; extruded strands, and great care in the drilling, trimming, and setting of the strands in the burner, I was able to hold the scatter of data in a complete burning rate versus pressure curve (30-1500 psig) to 1% standard deviation. That is, the standard deviation at any test pressure divided by the average burning rate from 5 runs at that pressure was 1% or less, which is well within the identifiable random errors.

APPENDIX V: Grain Construction and Motor Firing Procedure•Grain Construction

Motor Firing Procedure: About fifteen minutes prior to firing, the grass area subjected to the rocket exhaust was wet down by a sprinkling system, to prevent fire. During this time the motor was prepared for firing. The combustion chamber was securely mounted in a pipe vise and the grain spacer, grain, and igniter were placed inside. From this point the test cell warning buzzer was activated to warn personnel of an impending motor test. The nozzle was then inserted in the nozzle plate holder, the holder screwed into the combustion chamber, and tightened with a wrench. It was found that a light coating of oil on the sealing surfaces in contact with the metallic-asbestos gasket prevented seal surface scoring and insured a good gas seal. An electrical safety plug was then removed from the igniter firing circuit, cutting all electrical power to the circuit. This plug was then personally carried by the operator during all further preparations for firing and not reinserted in the circuit until the firing sequence was begun.

The prepared motor was then mounted on the thrustmount, the igniter wires connected to the igniter firing circuit, the exhaust product quencher put in place, and the water turned on. The exhaust product quencher was simply a one foot diameter, stainless steel tube with an internal water spray; its purpose was to absorb the gaseous HCl in the rocket exhaust to prevent adjacent personnel from breathing the fumes. The motor was then ready for the firing sequence and the personnel in adjacent test cells were warned of an impending test.

The igniter arming plug was inserted in the supply line from the 24V DC power source and the igniter power switch turned on, partially arming the igniter. The igniter power supply was then diverted through a

high resistance, causing 4.5 ma to flow through the igniter and register on a milliammeter on the control panel. This tested continuity in the igniter squib. A switch cutting out the high resistance was then turned on and the igniter circuit was fully armed, broken only by the normally open firing switch and the rocket was completely ready for testing, Figure 14.

Thirty seconds before closing the fire swtich, the test cell siren was turned on and at minus five seconds the Esterline-Angus chart drive was turned on. After thirty seconds of siren noise, the fire switch was closed, allowing 2 amperes to flow through the igniter and instantaneous ignition occured. After completion of the test, siren, warning buzzer, and exhaust product quencher were turned off. The motor was then allowed to cool and disassembled.

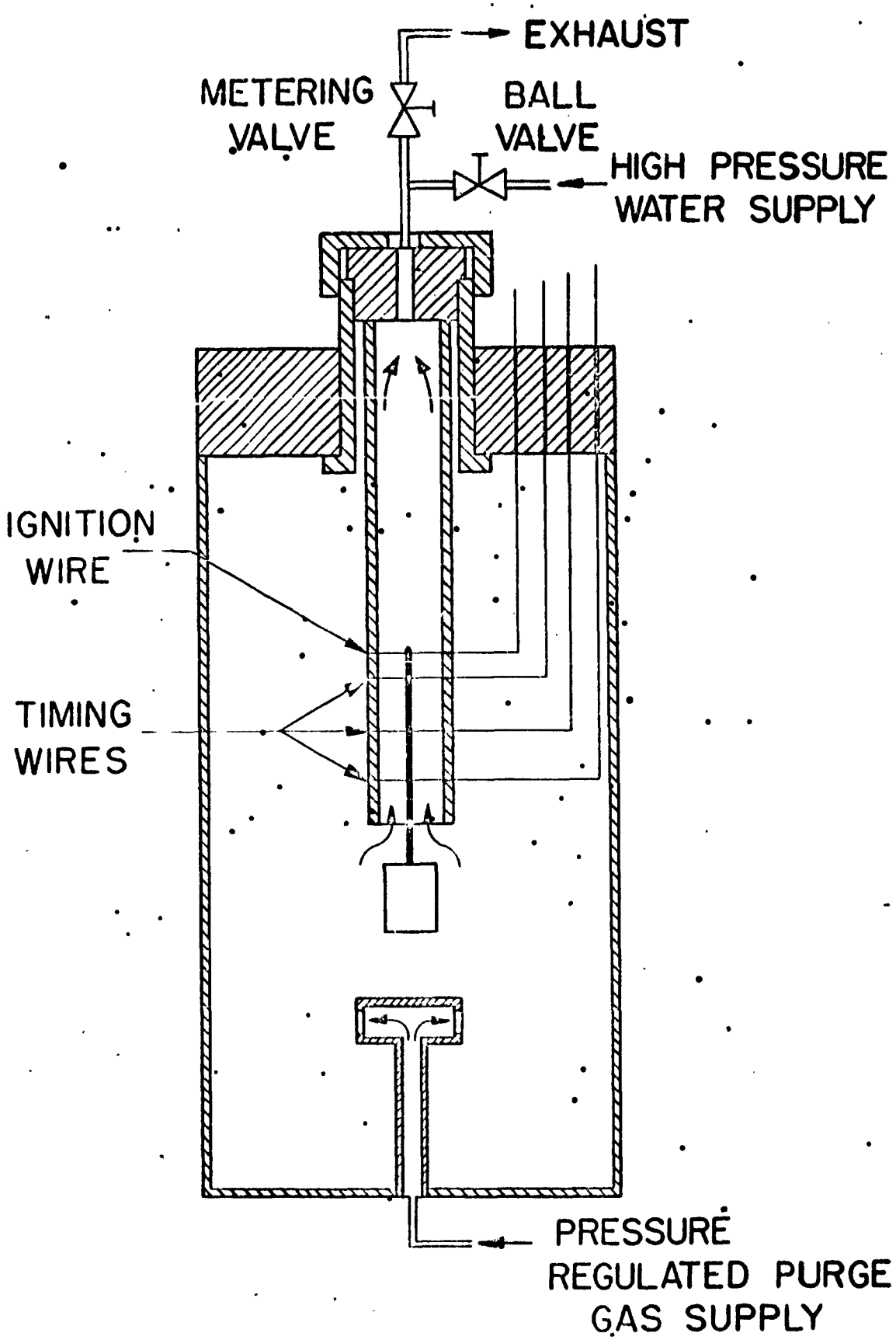

CHIMNEY STRAND BURNER

FIGURE 1

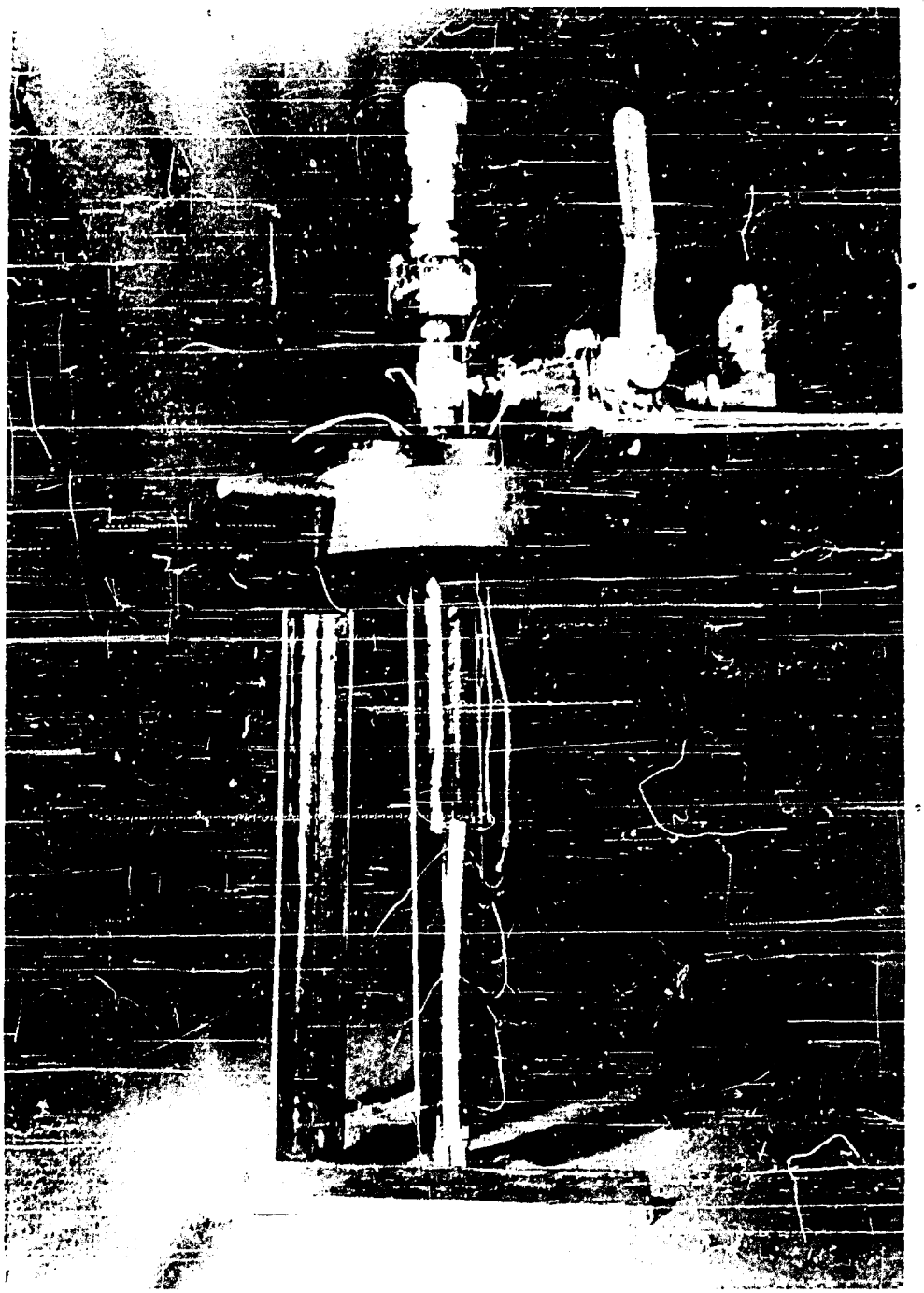

STRAND BURNER WITH STRAND IN PLACE

FIGURE 2

TYPICAL STRAND BURNING SURFACES, QUENCHED BURNING

FIGURE 3

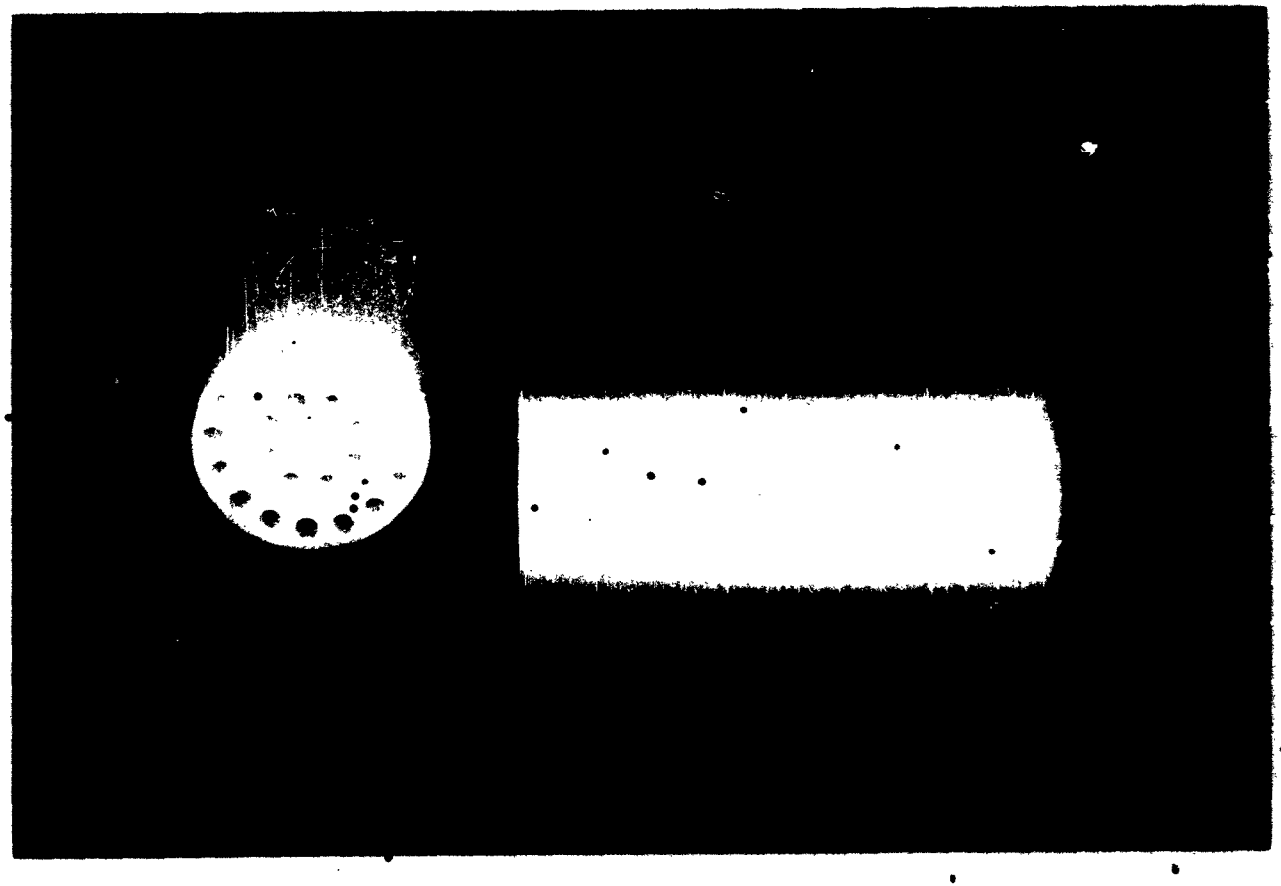

WAX MOLDS FOR EXTRUDED STRANDS

FIGURE 4

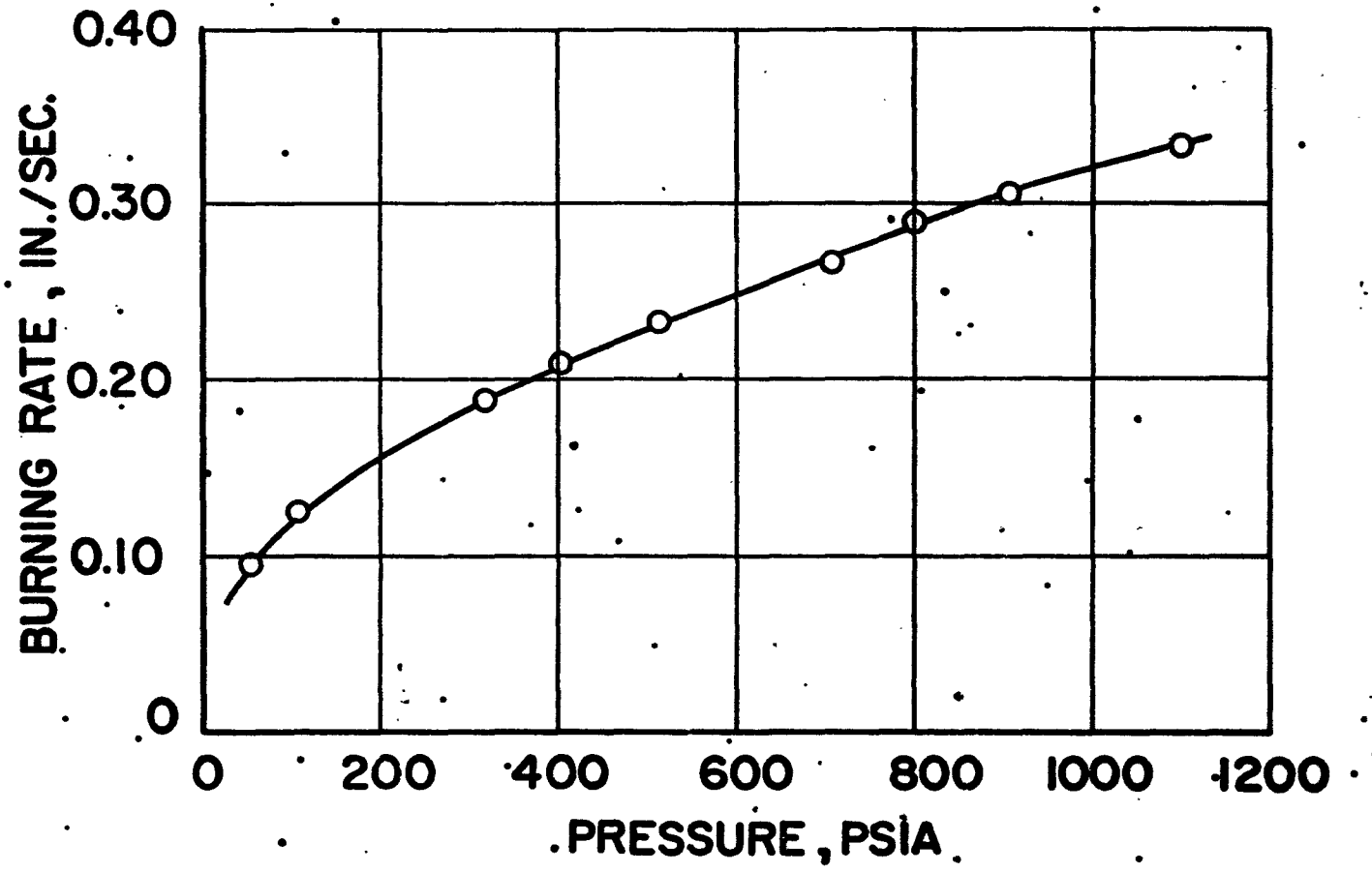

BURNING RATE VERSUS PRESSURE FOR STRANDS OF AP80:20 ROCKET MOTOR PROPELLANT

FIGURE 5

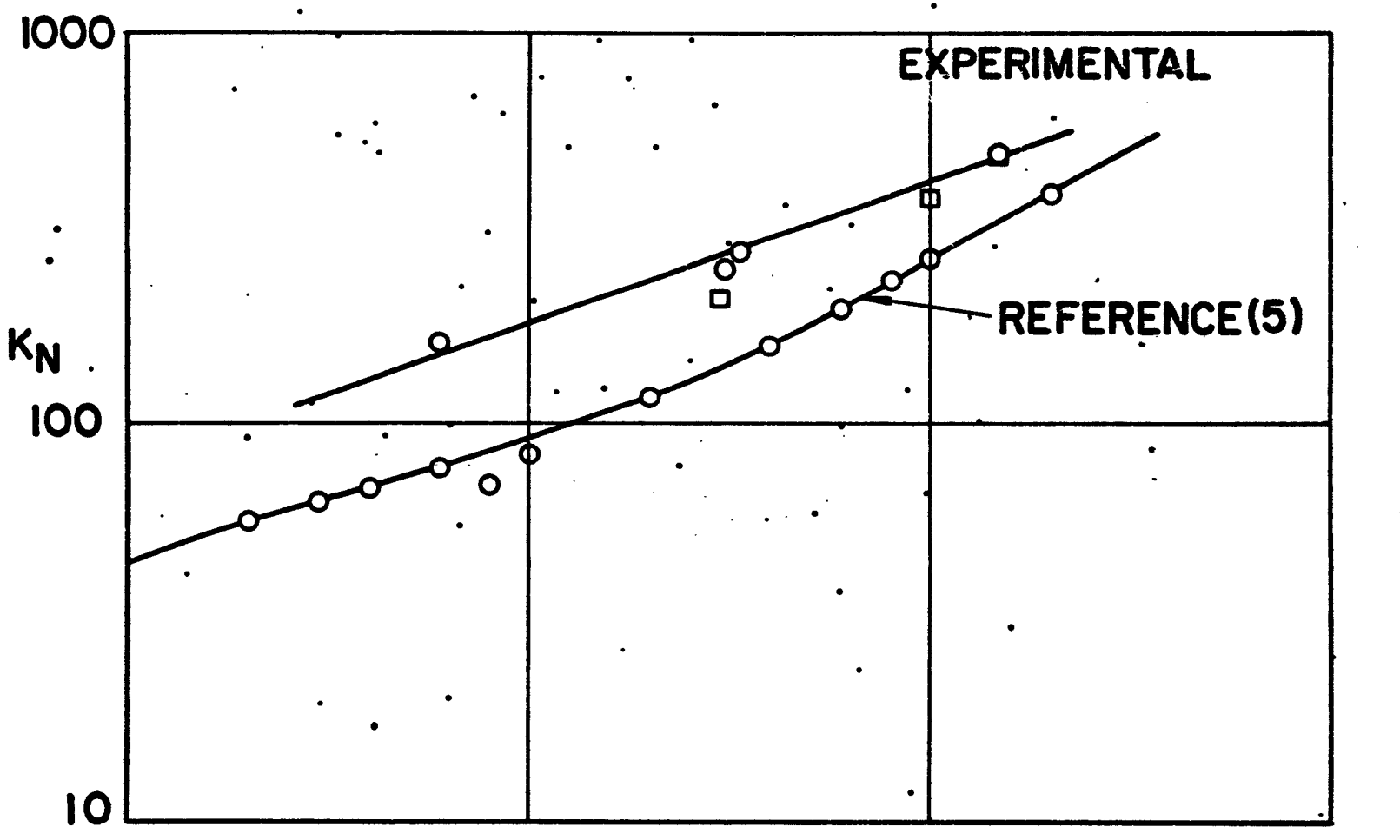

FIGURE 6

K_N vs $P_{CHAMBER}$ CURVE

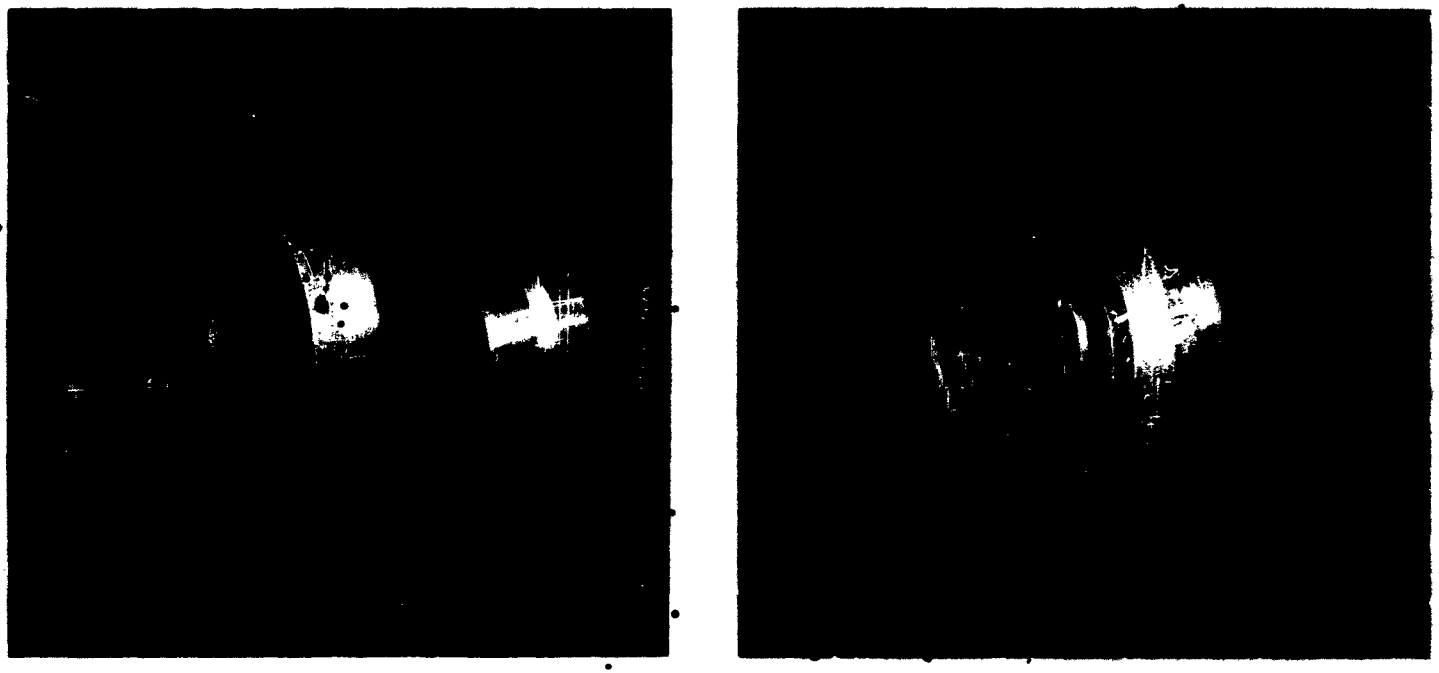

NOZZLE ASSEMBLY AND TYPICAL NOZZLE

FIGURE 7

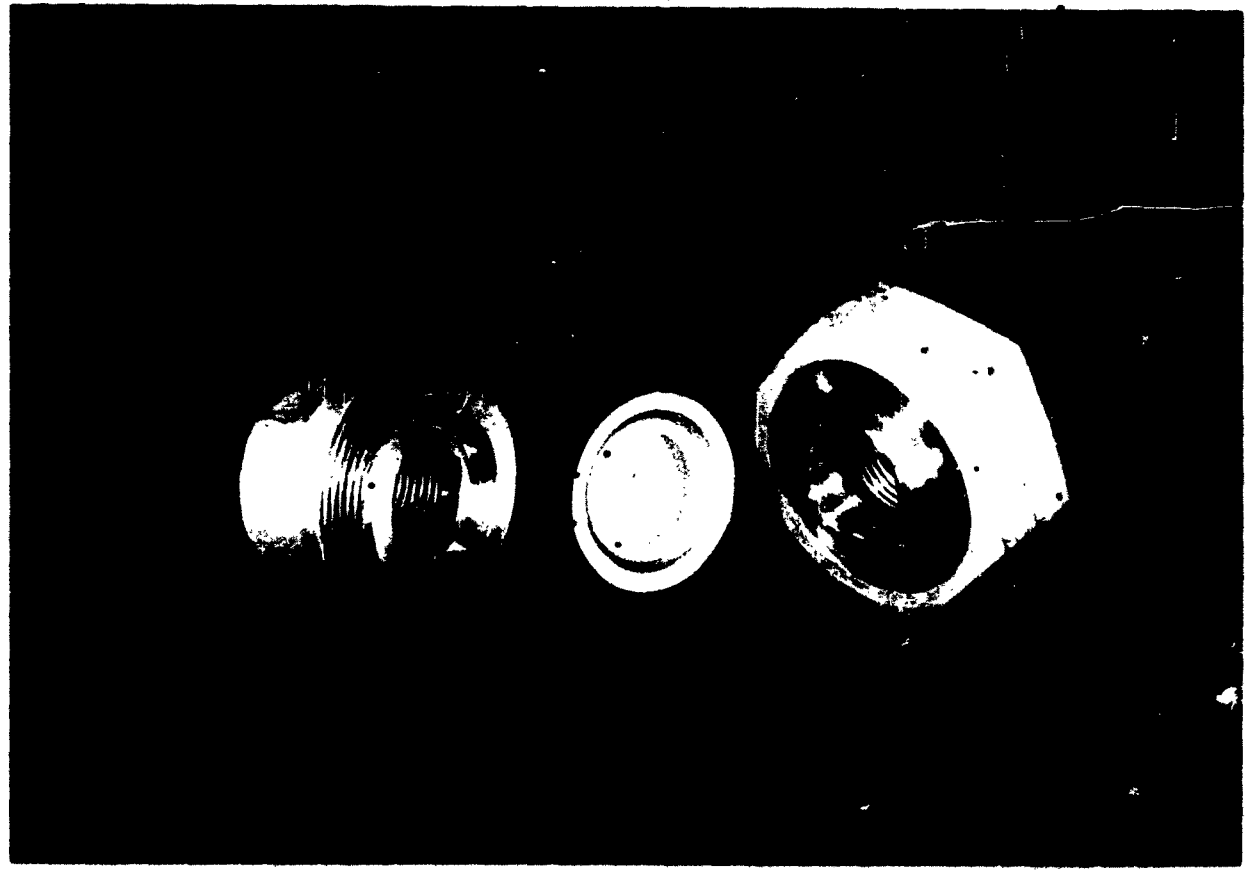

EXPLODED VIEW OF BURST DISC ASSEMBLY

FIGURE 8

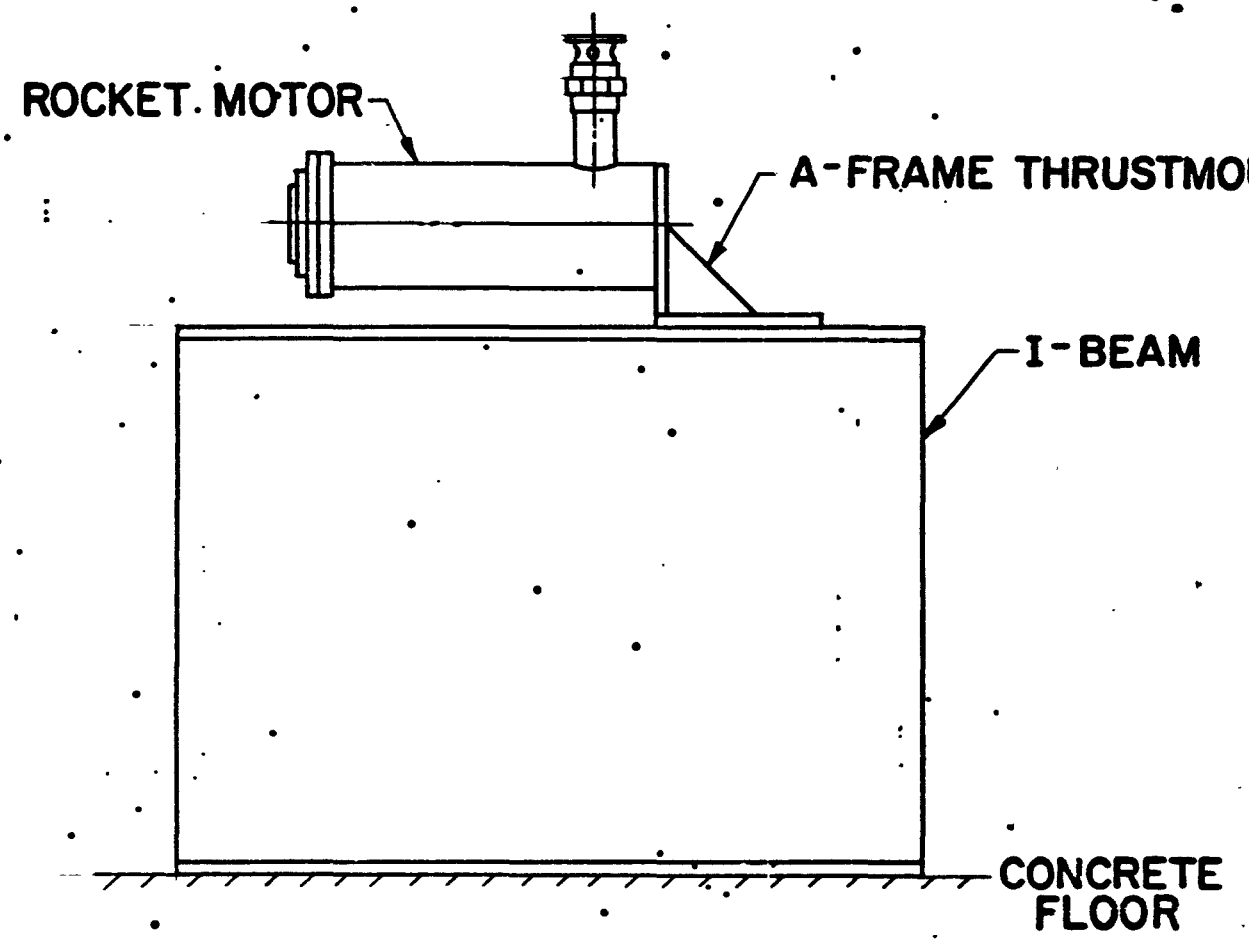

THRUSTMOUNT ASSEMBLY

FIGURE 9

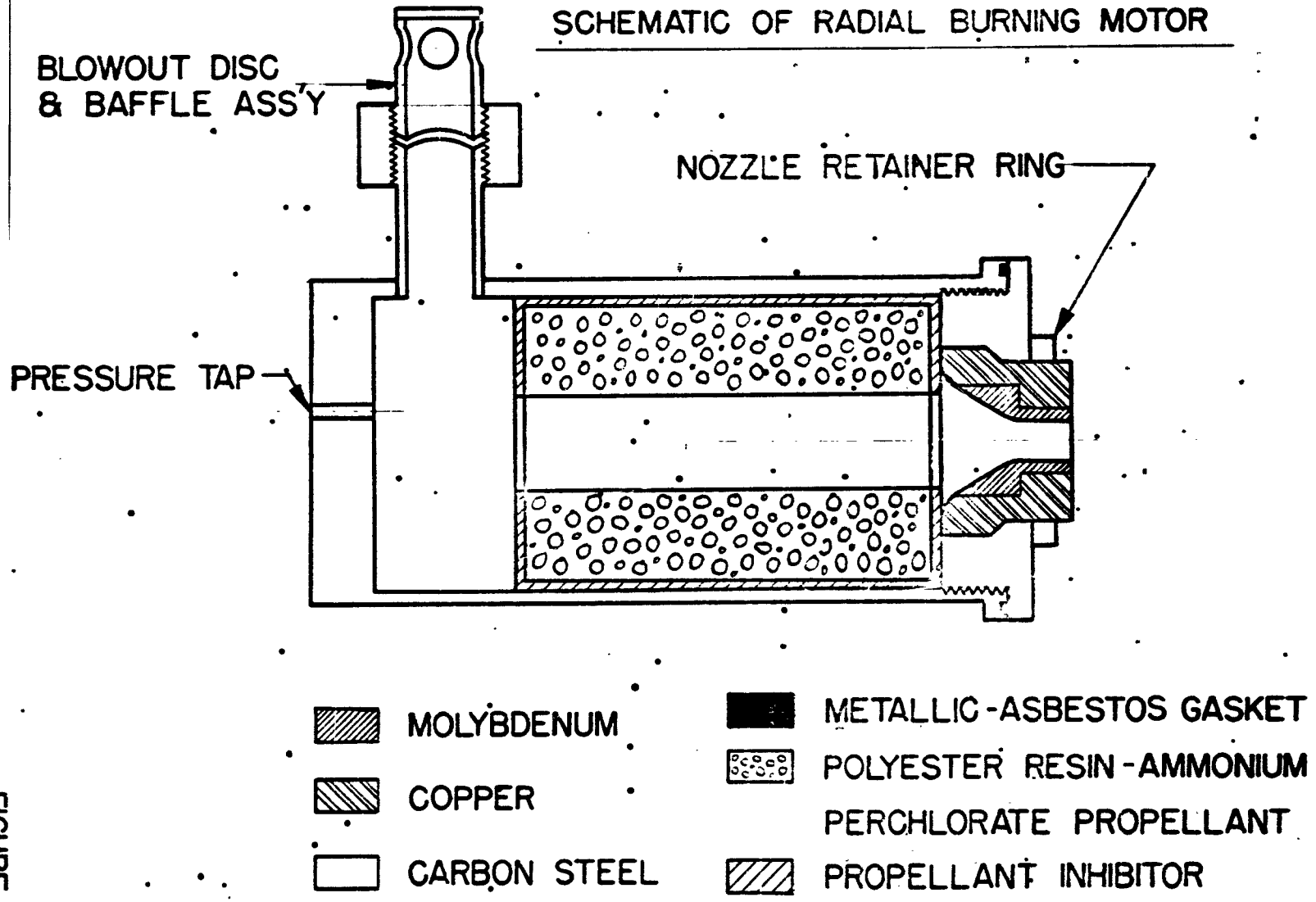
SCHEMATIC OF RADIAL BURNING MOTOR
BLOWOUT DISC
& BAFFLE ASS'Y
NOZZLE RETAINER RING
PRESSURE TAP
MOLYBDENUM
COPPER
CARBON STEEL
METALLIC-ASBESTOS GASKET
POLYESTER RESIN-AMMONIUM
PERCHLORATE PROPELLANT
PROPELLANT INHIBITOR

FIGURE 10

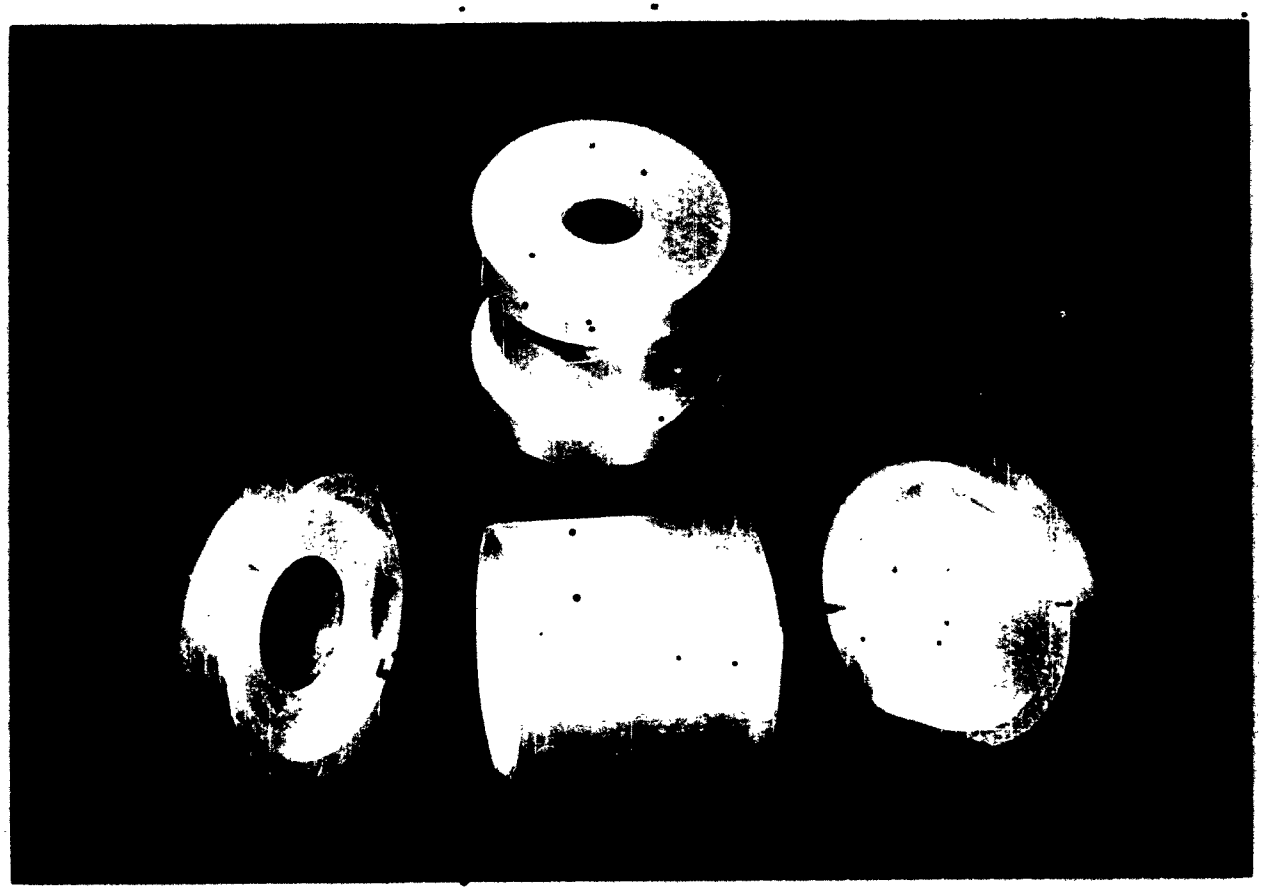

GRAIN MOLDS; EXPLODED AND ASSEMBLED MOLDS

FIGURE 11

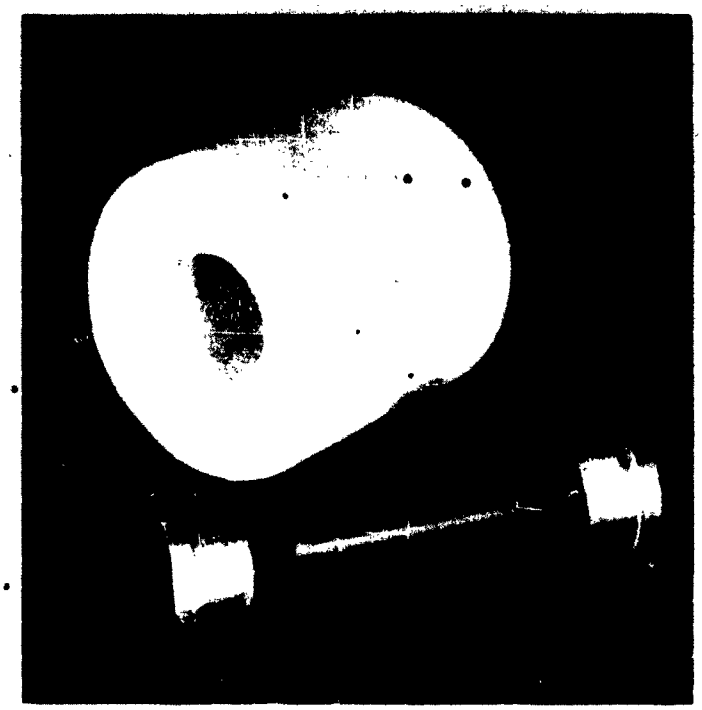

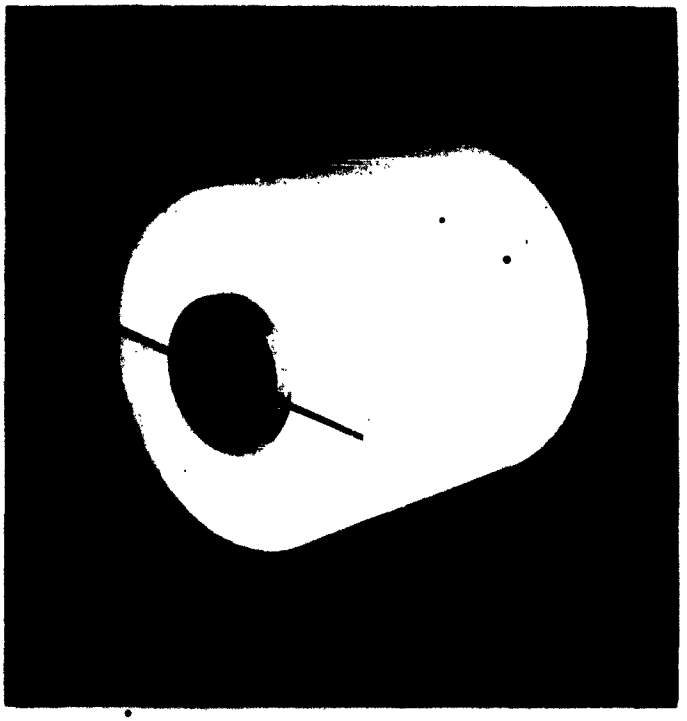

GRAIN PORT PLUGS - BEFORE AND AFTER INSTALLATION IN GRAIN

FIGURE 12

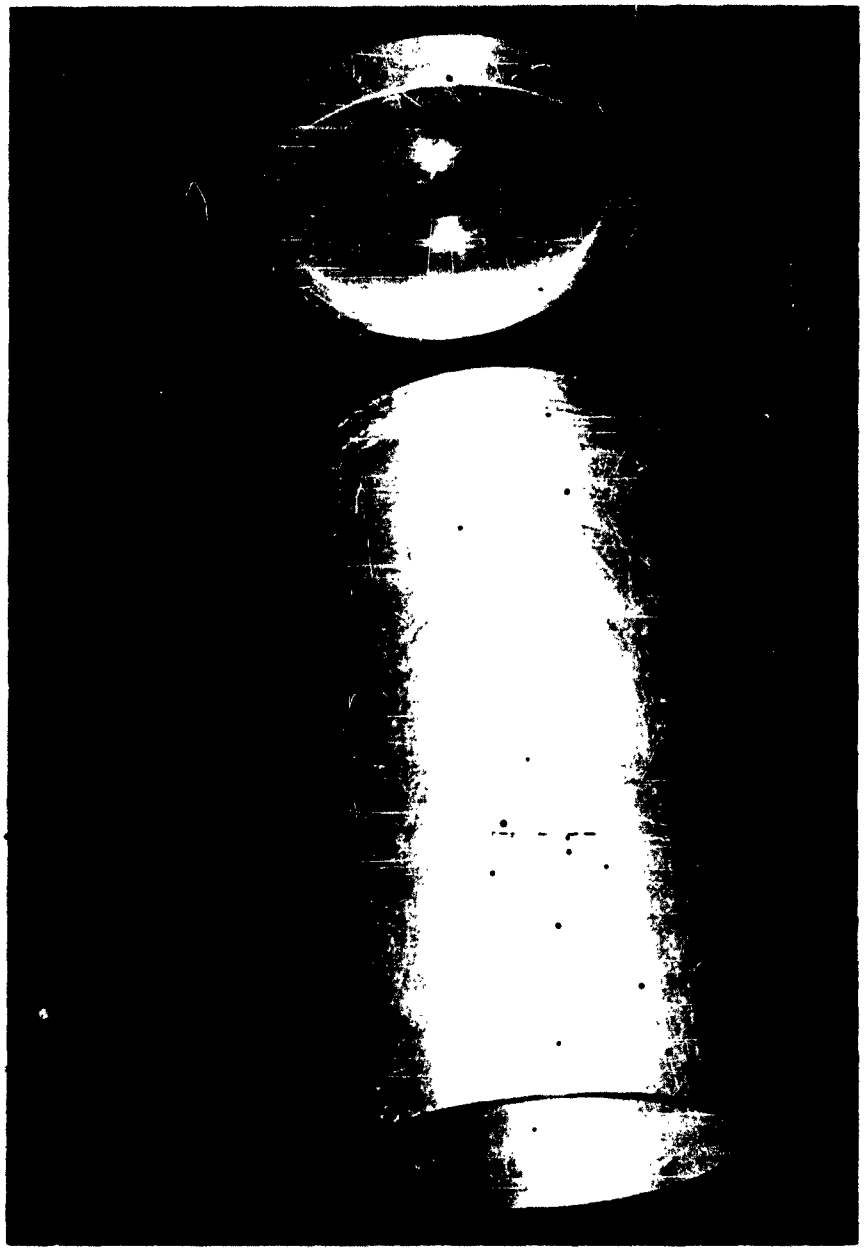

INHIBITOR MOLD

FIGURE 13

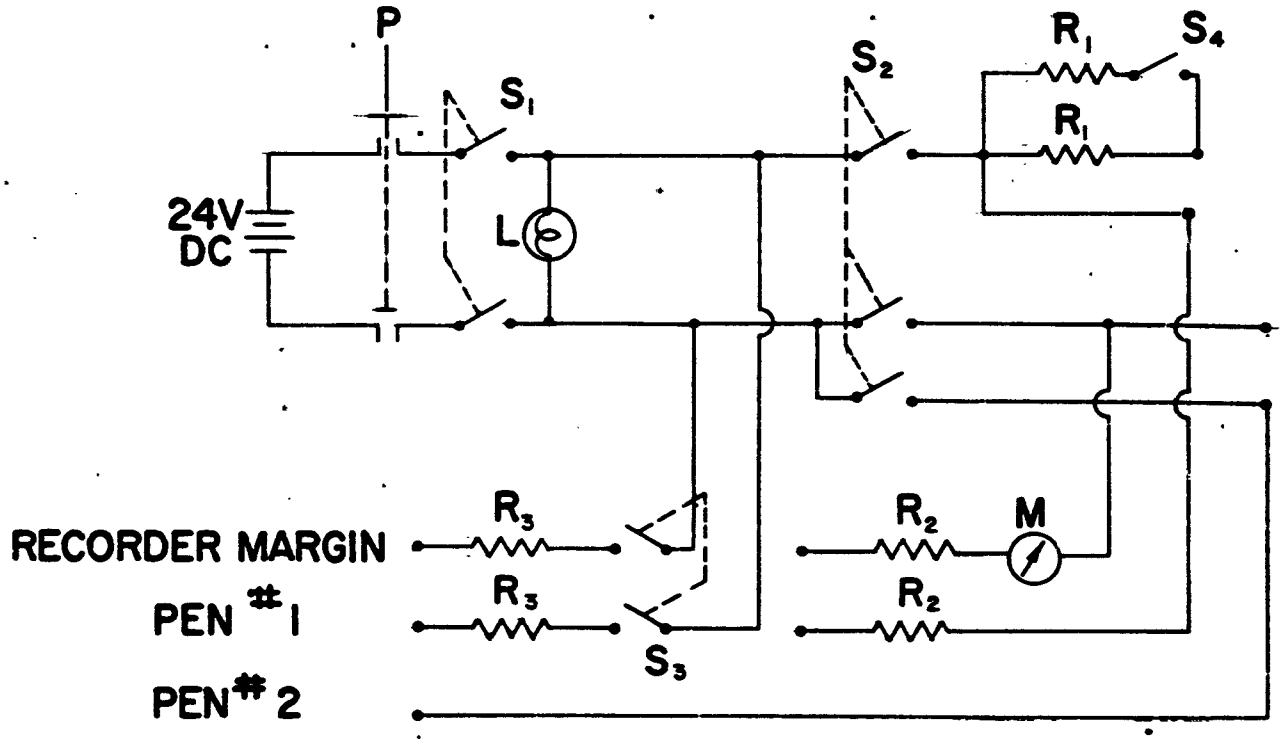

SWITCHES	RESISTORS	SYMBOLS
S_1 - DPST	R_1 - 11Ω, 44w	L - LAMP
S_2 - TPST	R_2 - 24Ω, 1w	M - MILLIAMMETER, 1 MA FULL SCALE
S_3 - DPDT	R_3 - 100Ω, 2w	P - SAFETY PLUG
S_4 - SPST		

FIGURE 14

IGNITER CIRCUIT SCHEMATIC

ROCKET MOTOR COMBUSTION
WATER QUENCH SYSTEM

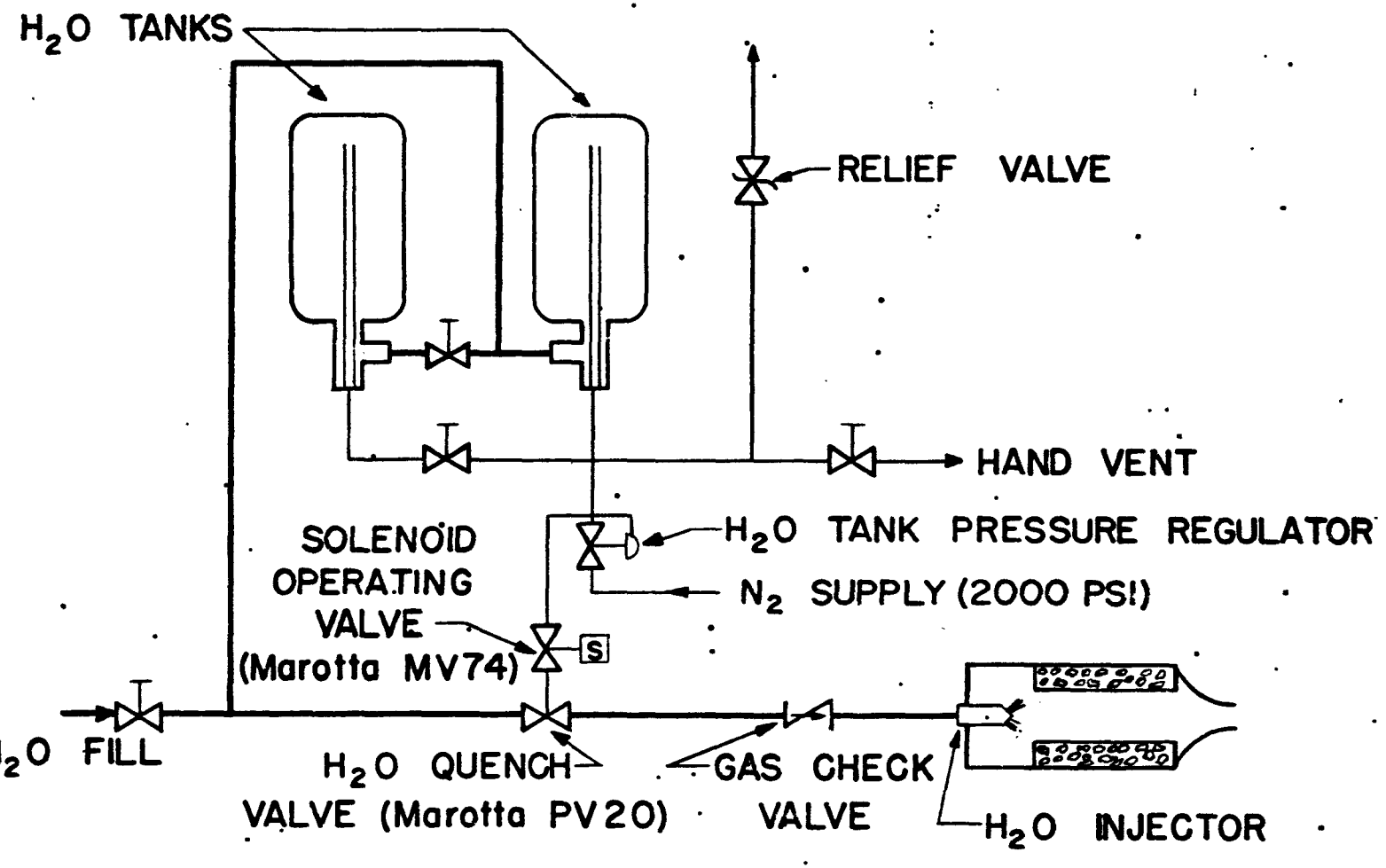

FIGURE 15

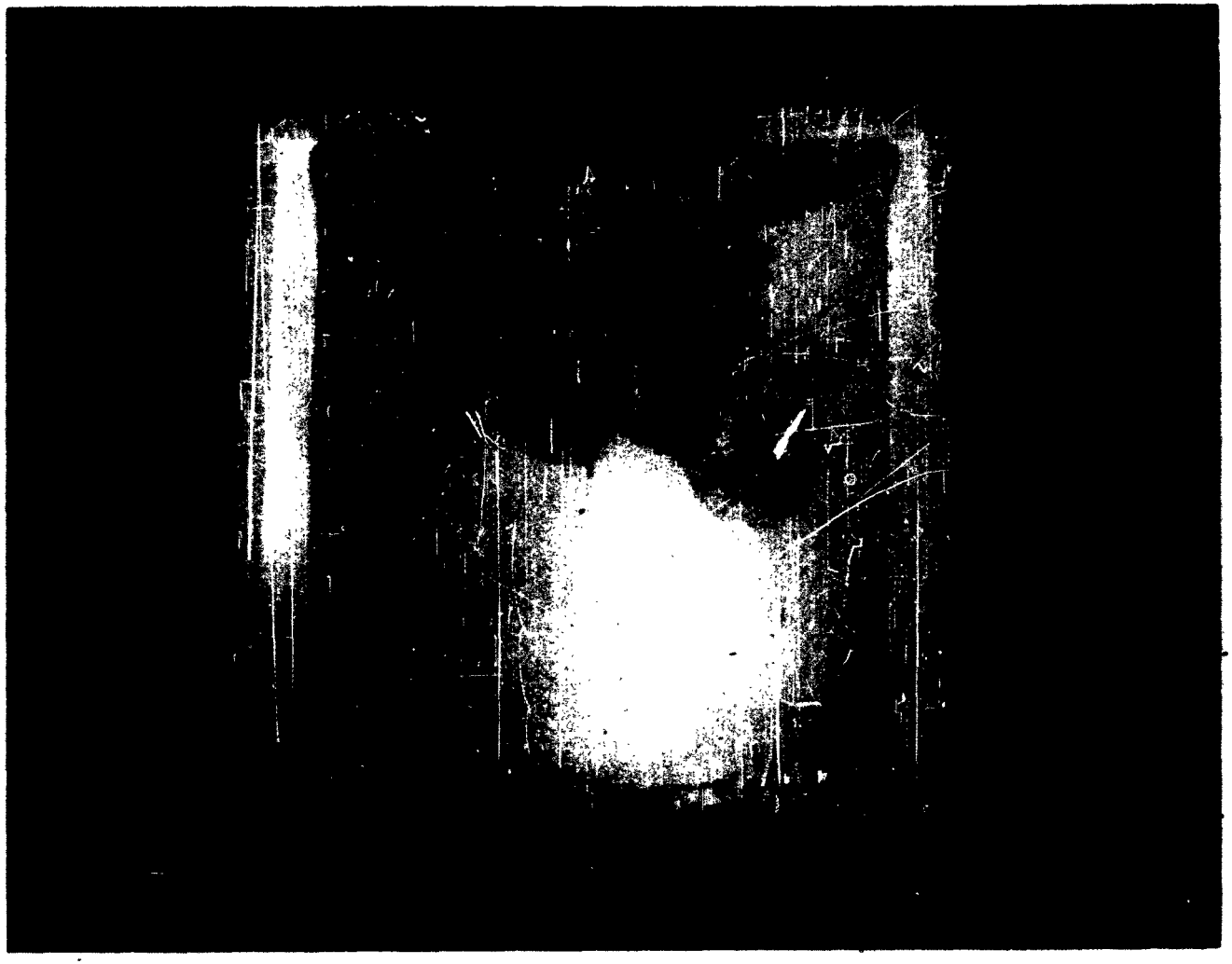

FIGURE 16

QUENCHED MOTOR GRAIN SHOWING BURNED HOLES

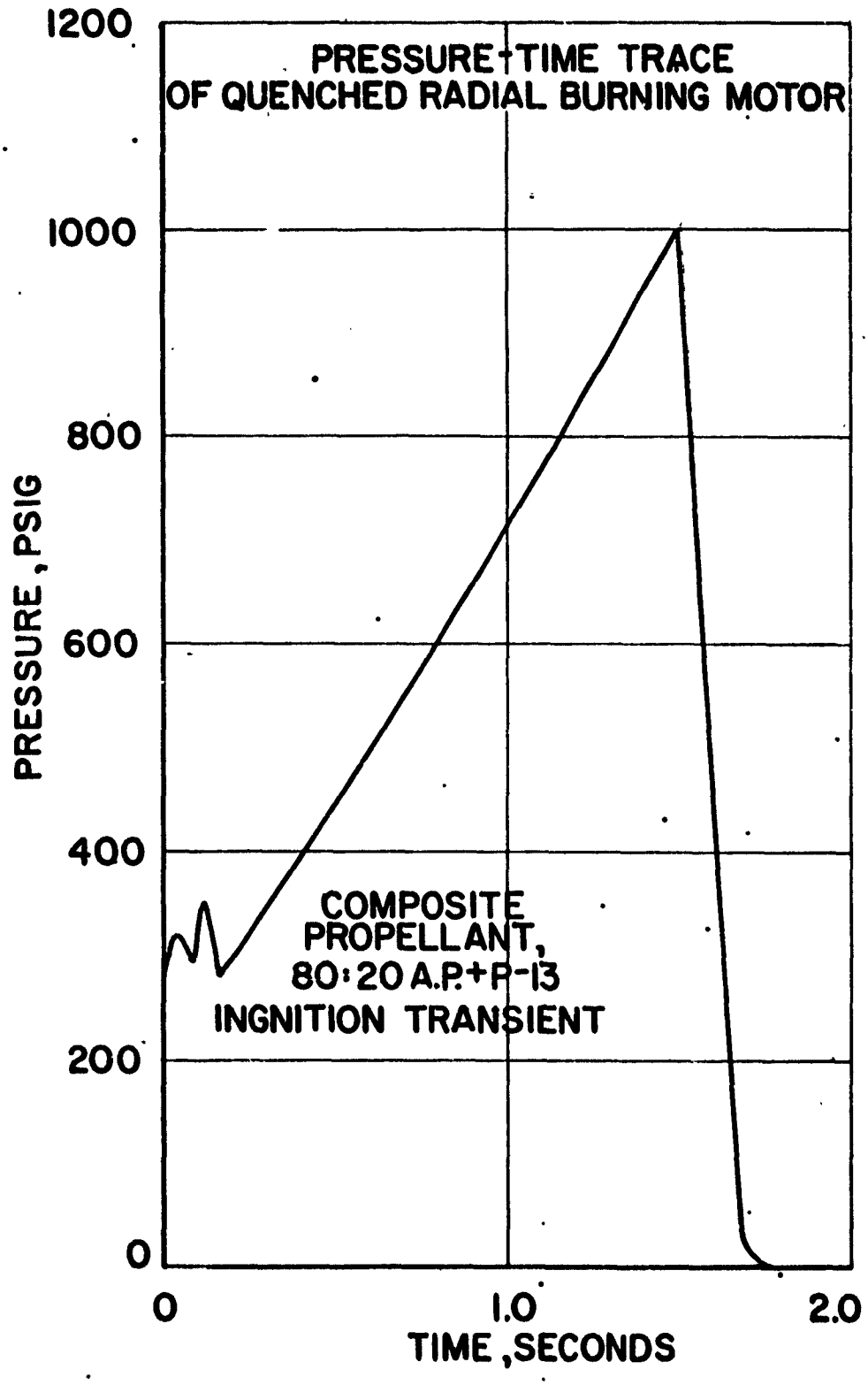
PRESSURE-TIME TRACE
OF QUENCHED RADIAL BURNING MOTOR
1200
1000
800
600
400
200
0
PRESSURE, PSIG
COMPOSITE
PROPELLANT,
80:20 A.P.+P-13
INGNITION TRANSIENT
0
1.0
2.0
TIME, SECONDS

FIGURE 17

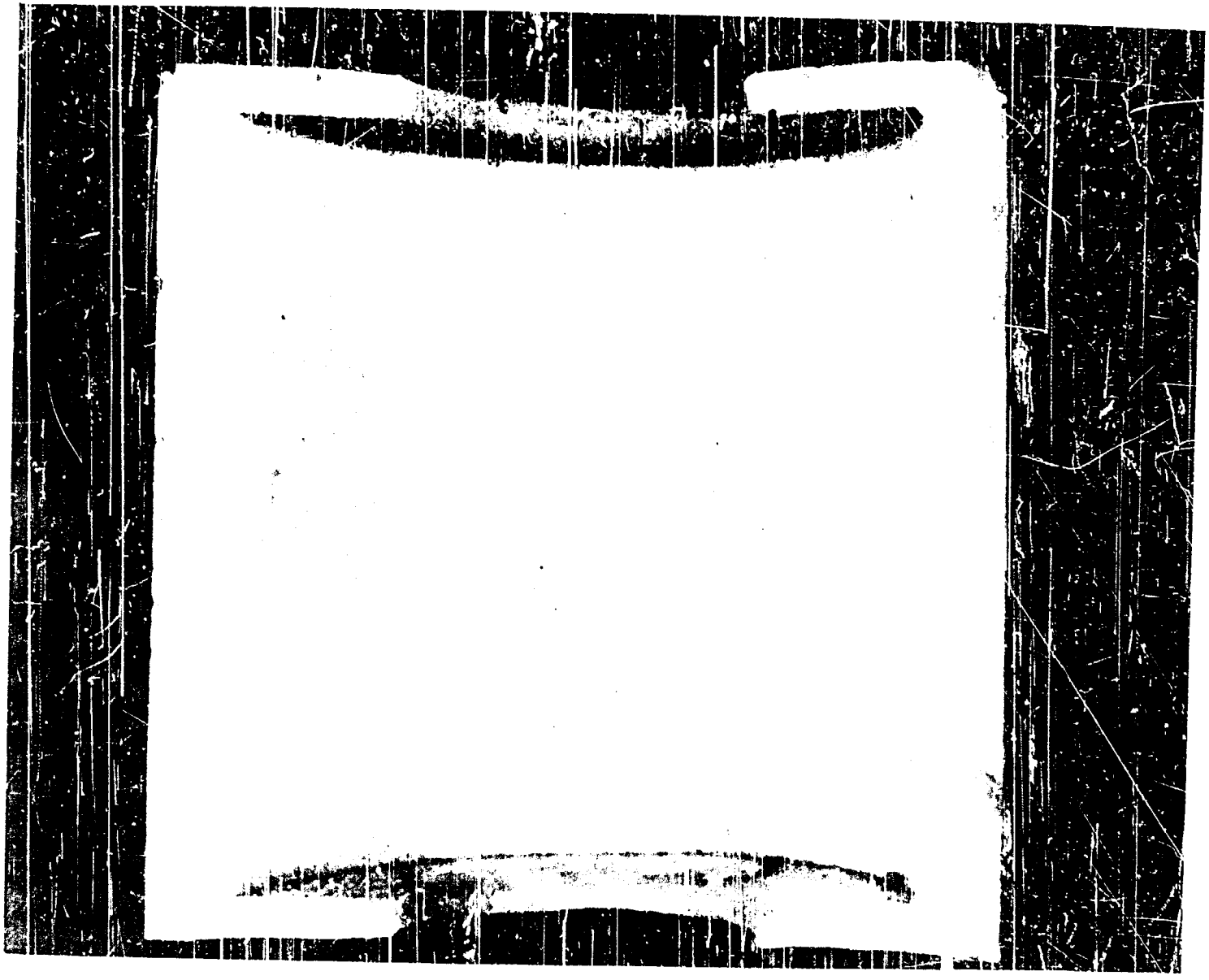

FIGURE 16

CLOSEUP PHOTOGRAPH OF QUENCHED GRAIN SHOWING INDENTATION OF BURNING SURFACE AT END OF GRAIN

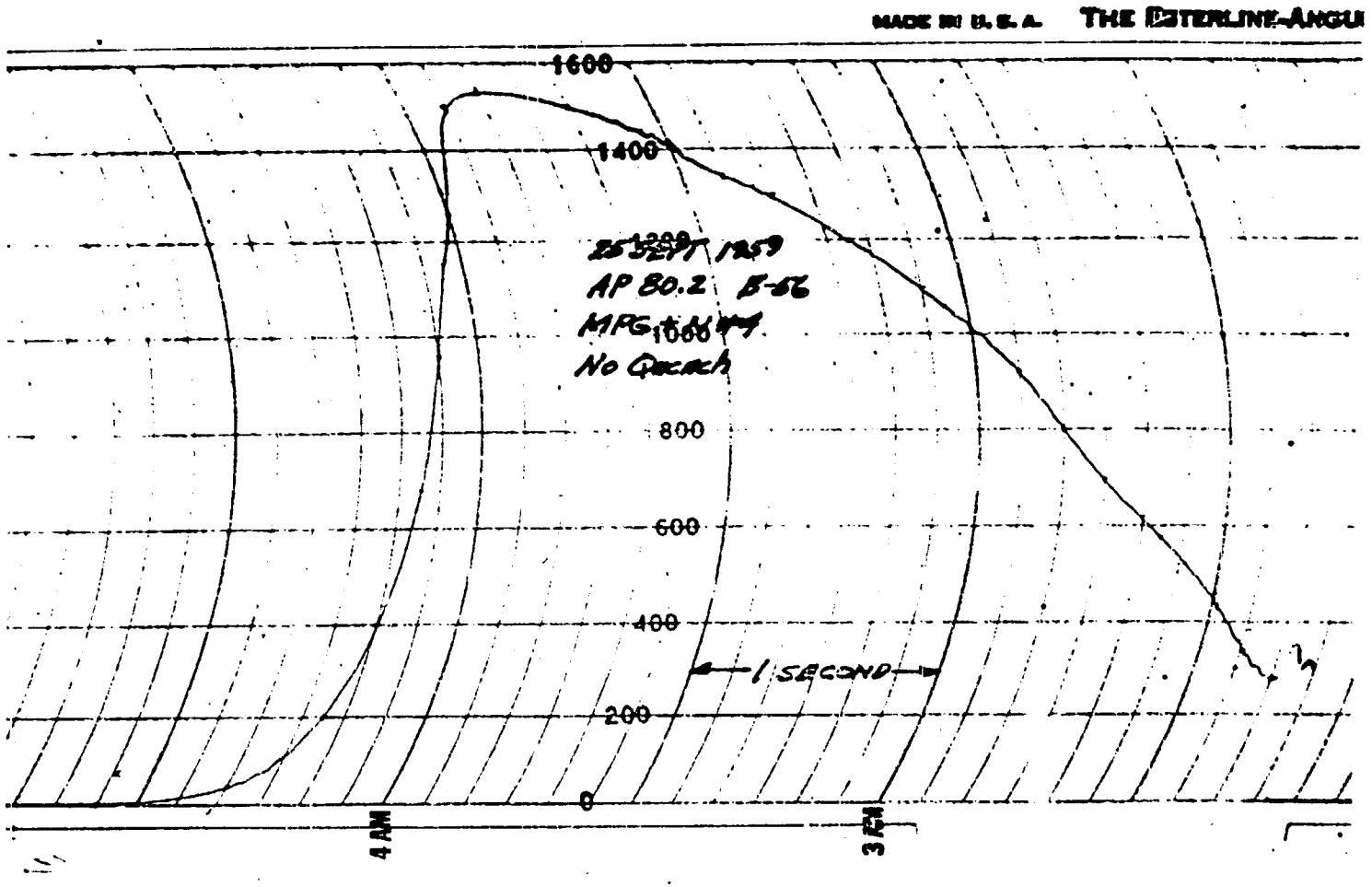

TYPICAL ROCKET MOTOR PRESSURE - TIME RECORDER RECORD

FIGURE 19

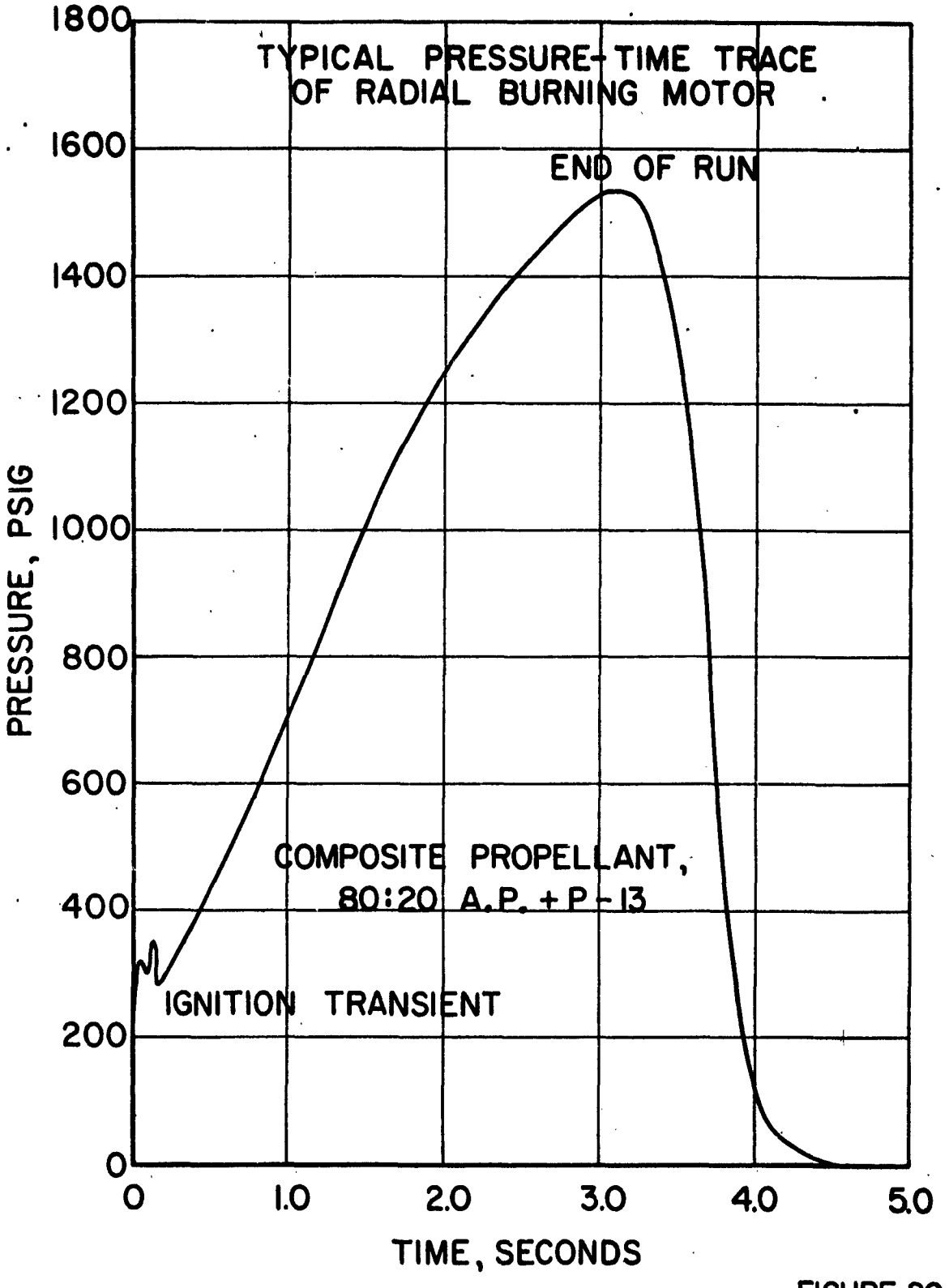
TYPICAL PRESSURE-TIME TRACE
OF RADIAL BURNING MOTOR
END OF RUN
COMPOSITE PROPELLANT,
80:20 A.P. + P-13
IGNITION TRANSIENT
PRESSURE, PSIG
1800
1600
1400
1200
1000
800
600
400
200
0
0
1.0
2.0
3.0
4.0
5.0
TIME, SECONDS

FIGURE 20

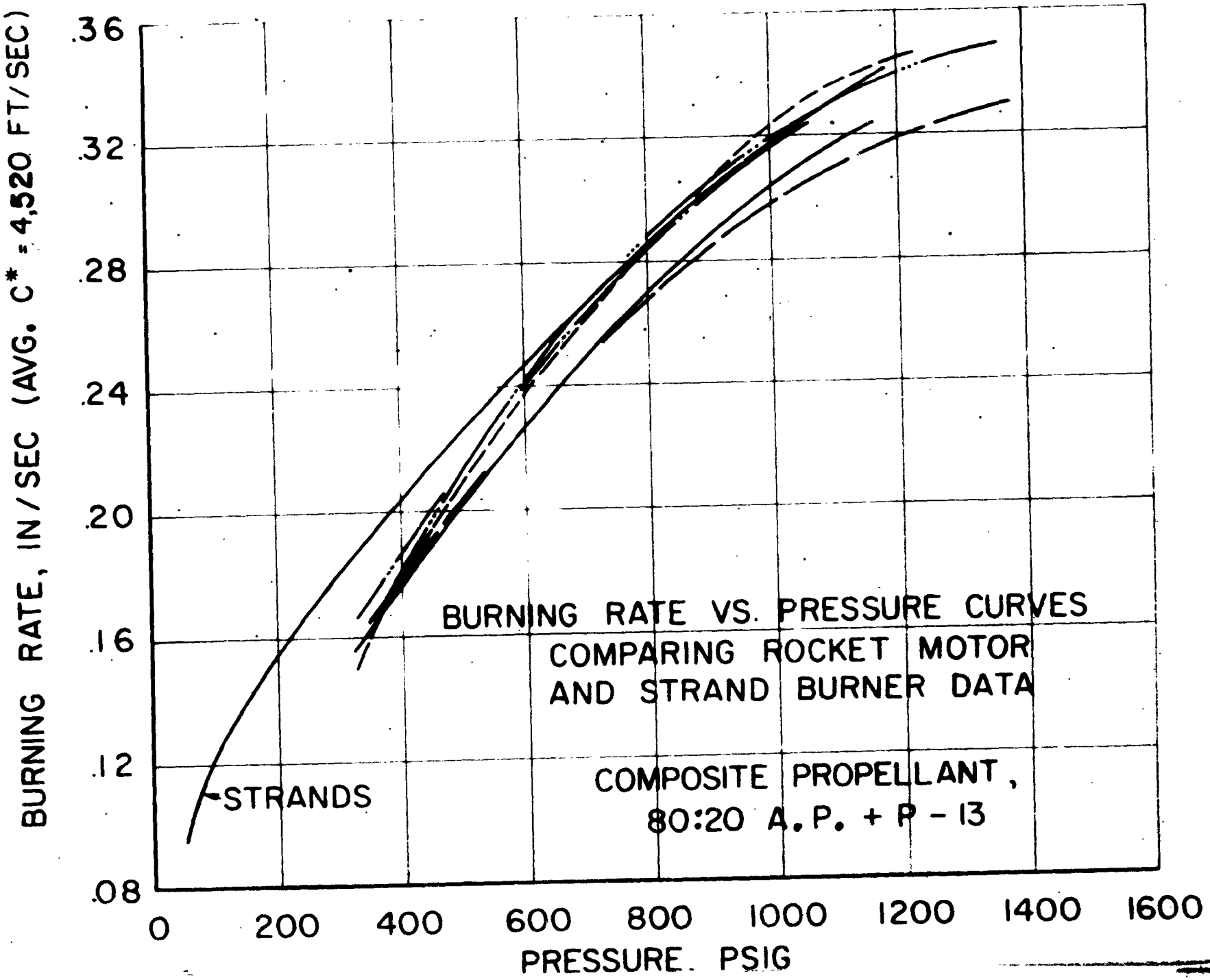
BURNING RATE, IN/SEC (AVG. C* = 4,520 FT/SEC)
.36
.32
.28
.24
.20
.16
.12
.08
0
200
400
600
800
1000
1200
1400
1600
PRESSURE. PSIG
BURNING RATE VS. PRESSURE CURVES
COMPARING ROCKET MOTOR
AND STRAND BURNER DATA
COMPOSITE PROPELLANT,
80:20 A.P. + P-13
STRANDS

FIGURE 21

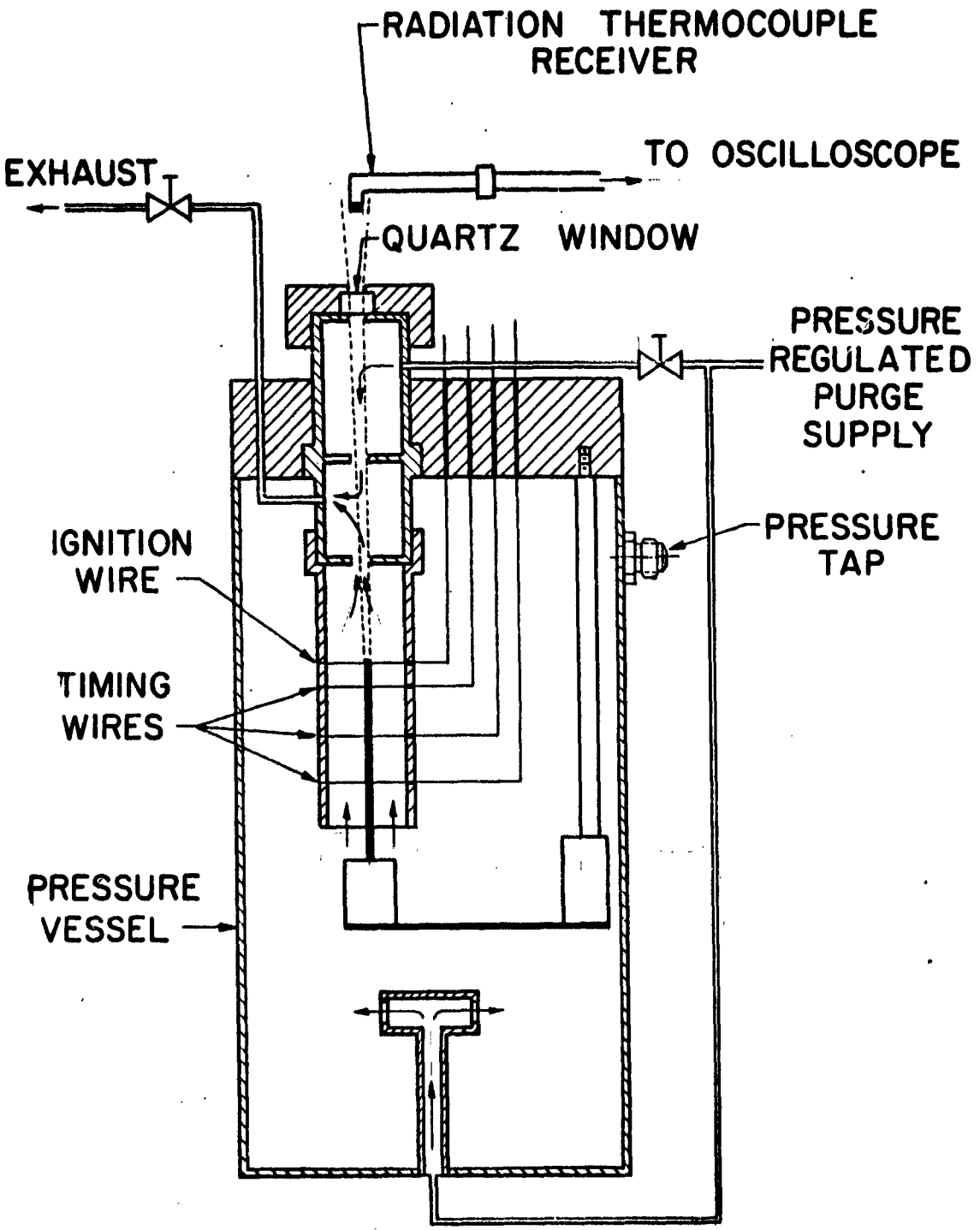

STRAND BURNER FOR RADIATION MEASUREMENT

FIGURE 22

SCHEMATIC OF RADIAL BURNING MOTOR
WITH RADIATION RECEIVER

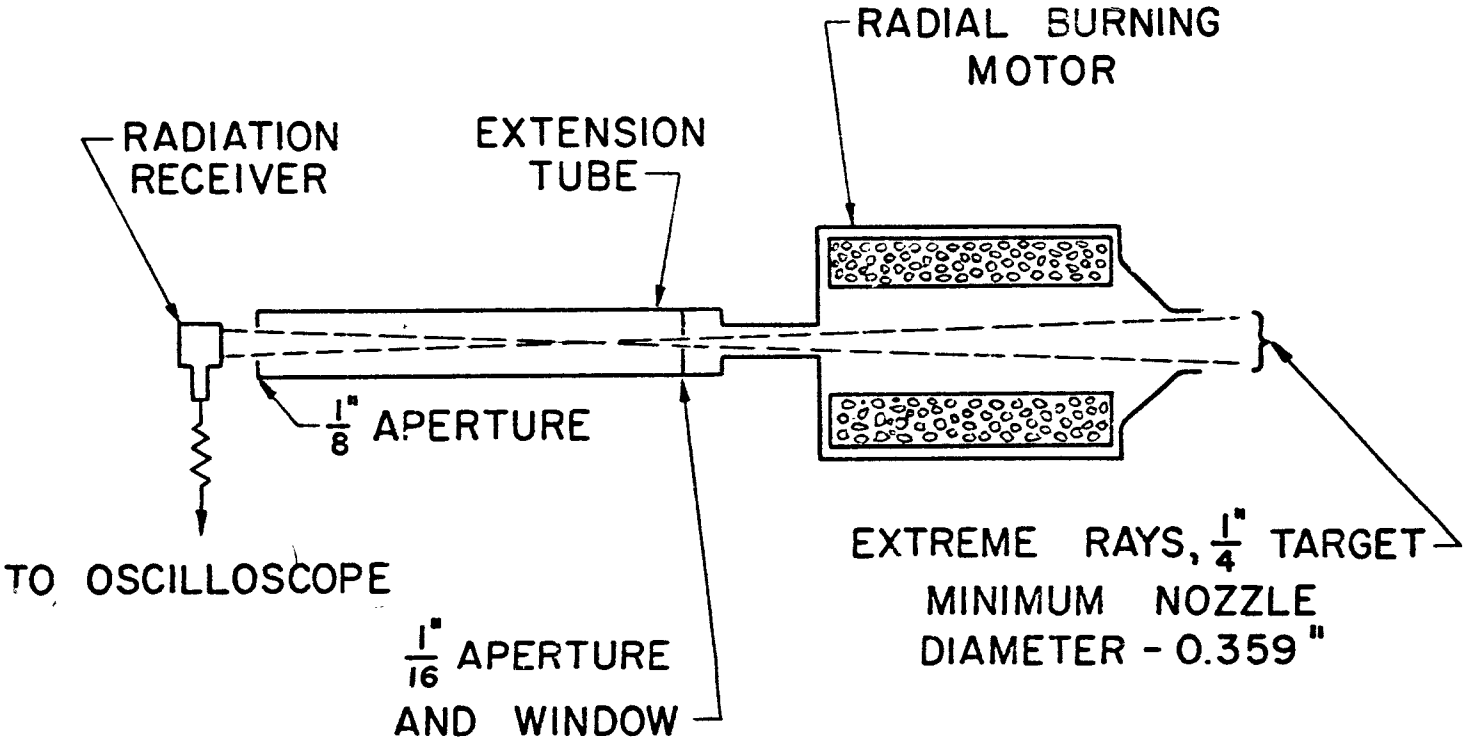

FIGURE 23

TYPICAL RADIATION INTENSITY TIME TRACE FROM ROCKET MOTOR RADIATION EXPERIMENTS (KBr OPTICS)

FIGURE 24